Molecular Cell

Article

Vesicle Tethering on the Surface of Phase-Separated Active Zone Condensates

Graphical Abstract

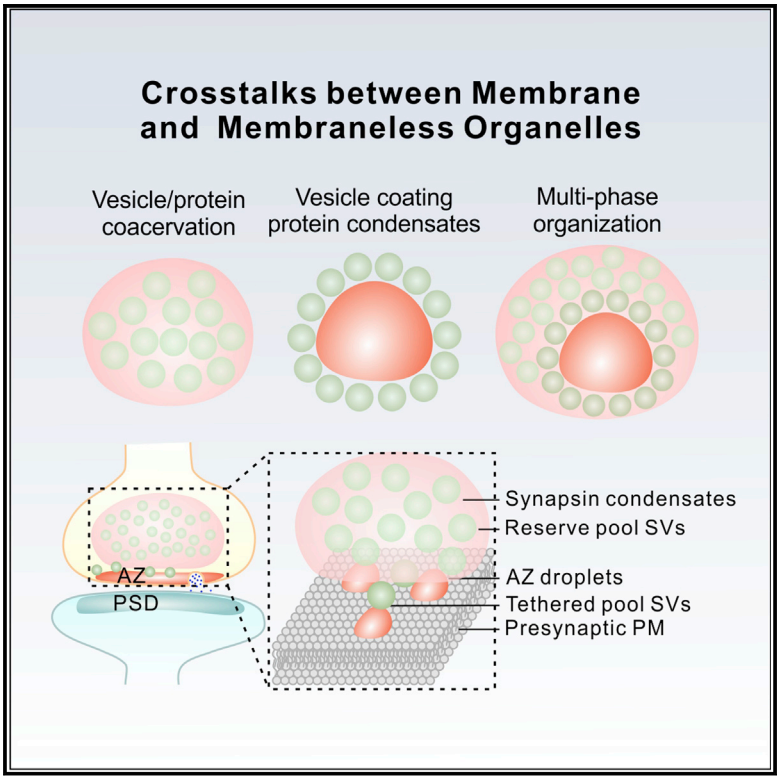

Authors

Xiandeng Wu, Marcelo Ganzella, Jinchuan Zhou, Shihan Zhu, Reinhard Jahn, Mingjie Zhang

Correspondence

mzhang@ust.hk

In Brief

Each presynaptic bouton contains reserve pool synaptic vesicles (SVs) and a few active zone-tethered SVs. Wu et al. show that SVs coat the surface of protein condensates formed by active zone proteins, such as RIM, RIM-BP, and ELKS, but coacervate with synapsin, forming a multi-phase organization with the docked pool SVs surrounded by the bulk reserve pool SVs as observed in presynaptic boutons.

Highlights

- Synaptic vesicles coat active zone condensate but coacervate with synapsin condensate
- SV/synapsin co-condensates encapsulate SV-coated active zone condensates
- A presynaptic bouton-like assembly with reserve and tethered SV pools is reconstituted
- Membraneless condensates and membrane organelles can interact with distinct modes

Wu et al., 2021, Molecular Cell *81*, 1–12
January 7, 2021
https://doi.org/10.1016/j.molcel.2020.10.029

CellPress

Please cite this article in press as: Wu et al., Vesicle Tethering on the Surface of Phase-Separated Active Zone Condensates, Molecular Cell (2020), https://doi.org/10.1016/j.molcel.2020.10.029

Molecular Cell

CellPress

Article

Vesicle Tethering on the Surface of Phase-Separated Active Zone Condensates

Xiandeng Wu,[1] Marcelo Ganzella,[2] Jinchuan Zhou,[1,3] Shihan Zhu,[1] Reinhard Jahn,[2] and Mingjie Zhang[1,4,5,*]

[1]Division of Life Science, State Key Laboratory of Molecular Neuroscience, Hong Kong University of Science and Technology, Clear Water Bay, Kowloon, Hong Kong, China

[2]Department of Neurobiology, Max Planck Institute for Biophysical Chemistry, Göttingen 37077, Germany

[3]Institute for Advanced Study, Hong Kong University of Science and Technology, Clear Water Bay, Kowloon, Hong Kong, China

[4]Center of Systems Biology and Human Health, Hong Kong University of Science and Technology, Clear Water Bay, Kowloon, Hong Kong, China

[5]Lead Contact

*Correspondence: mzhang@ust.hk

https://doi.org/10.1016/j.molcel.2020.10.029

SUMMARY

Tethering of synaptic vesicles (SVs) to the active zone determines synaptic strength, although the molecular basis governing SV tethering is elusive. Here, we discover that small unilamellar vesicles (SUVs) and SVs from rat brains coat on the surface of condensed liquid droplets formed by active zone proteins RIM, RIM-BP, and ELKS via phase separation. Remarkably, SUV-coated RIM/RIM-BP condensates are encapsulated by synapsin/SUV condensates, forming two distinct SUV pools reminiscent of the reserve and tethered SV pools that exist in presynaptic boutons. The SUV-coated RIM/RIM-BP condensates can further cluster Ca^{2+} channels anchored on membranes. Thus, we reconstitute a presynaptic bouton-like structure mimicking the SV-tethered active zone with its one side attached to the presynaptic membrane and the other side connected to the synapsin-clustered SV condensates. The distinct interaction modes between membraneless protein condensates and membrane-based organelles revealed here have general implications in cellular processes, including vesicular formation and trafficking, organelle biogenesis, and autophagy.

INTRODUCTION

Active zones in presynaptic terminal boutons of synapses are intimately involved in neurotransmitter release, because active zones are responsible for tethering and docking synaptic vesicles (SVs) to be near release sites at plasma membranes, priming SVs for action potential-evoked fusion and clustering voltage-gated Ca^{2+} channels (VGCCs) for precise spatiotemporal control of Ca^{2+} level at the release sites (Biederer et al., 2017; Jahn and Fasshauer, 2012; Südhof, 2012, 2013). Electron microscopy and super-resolution optical imaging experiments have shown that active zone proteins, including RIM, RIM-BP, ELKS, Munc13, and Liprin, are located within a narrow space of <100 nm from the presynaptic terminal membranes (Dani et al., 2010; Glebov et al., 2017; Kittel et al., 2006; Limbach et al., 2011; Liu et al., 2011; Sakamoto et al., 2018; Tang et al., 2016; Wilhelm et al., 2014; Wong et al., 2018). Biochemically, these active zone proteins are all multi-domain scaffold proteins without intrinsic enzymatic activities, and these proteins can form an intricate molecular network by specific protein-protein interactions (Ackermann et al., 2015; Haucke et al., 2011; Schoch and Gundelfinger, 2006; Südhof, 2012; Ziv and Garner, 2004), suggesting that active zones are large and dense protein-based molecular assemblies. Such active zone assemblies were proposed to be anchored to presynaptic plasma membranes by directly binding to lipids or transmembrane proteins, such as LAR and VGCCs (Biederer et al., 2017; Chen et al., 2011; Emperador-Melero and Kaeser, 2020; Um and Ko, 2013), but none of them alone has been proved to be essential (Emperador-Melero and Kaeser, 2020; Held et al., 2020; Sclip and Südhof, 2020). Genetic and cell biology studies have shown that these proteins function together and in redundant ways in organizing active zones and in modulating neurotransmitter releases. For example, removal of each active zone component in rodents individually showed little impact on the active zone structures and vesicle tethering to active zones, except that removal of RIM led to ~50% reduction of tethered vesicles (Han et al., 2011; Kaeser et al., 2011). Combined removals of RIM with RIM-BP or with ELKS led to disintegration of active zone molecular assemblies, near-total loss of vesicle tethering and docking, and dramatic impairments of synaptic release (Acuna et al., 2016; Wang et al., 2016).

We recently showed that RIM and RIM-BP, when mixed *in vitro*, can autonomously form condensed molecular assembly via phase separation. The RIM/RIM-BP condensates can cluster the cytosolic tail of VGCC (VGCC-CT) tethered to lipid membranes, forming highly concentrated RIM/RIM-BP/VGCC-CT

Please cite this article in press as: Wu et al., Vesicle Tethering on the Surface of Phase-Separated Active Zone Condensates, Molecular Cell (2020), https://doi.org/10.1016/j.molcel.2020.10.029

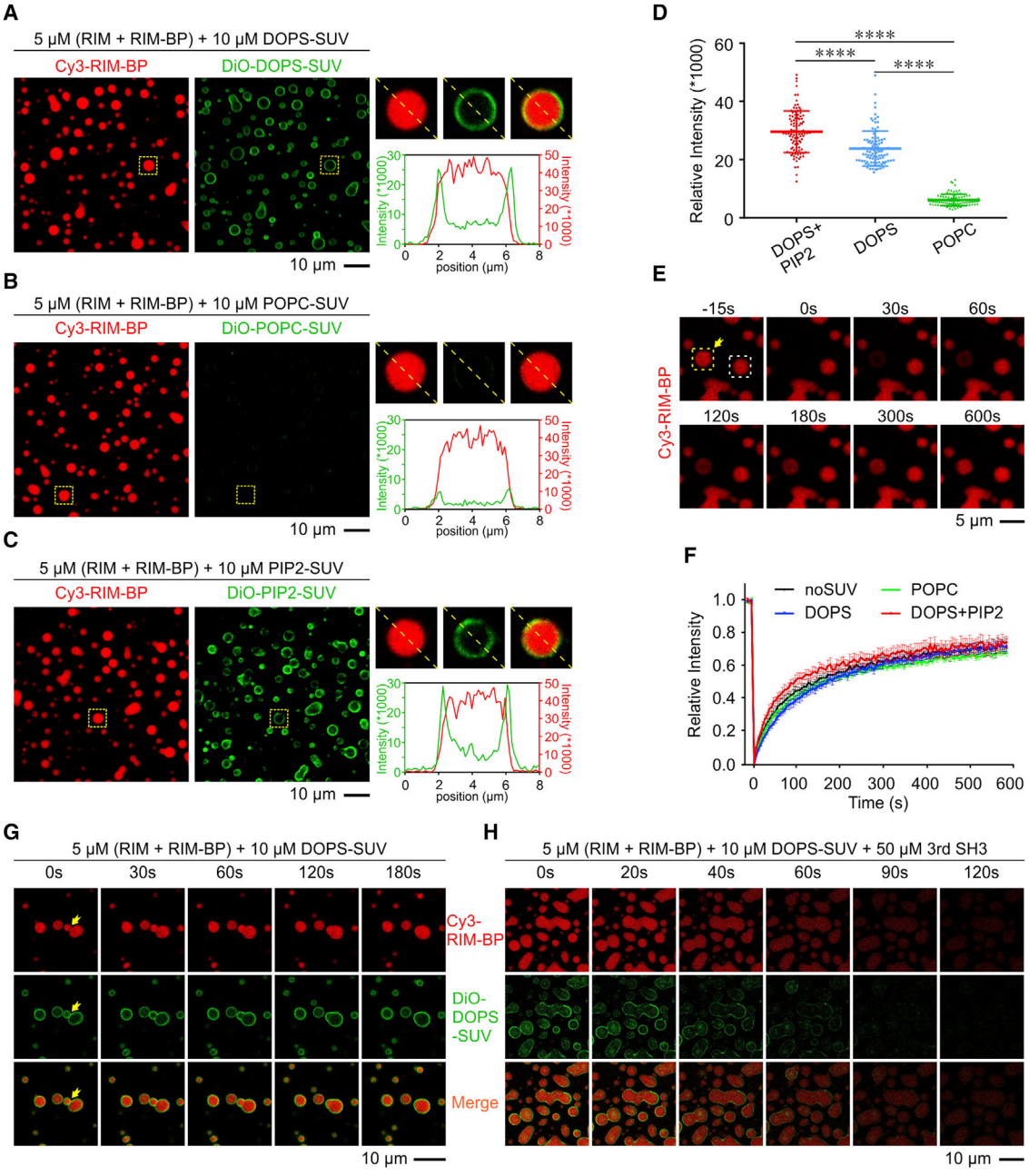

Figure 1. SUVs Coat on the Surface of the RIM/RIM-BP Condensates

(A–C) Negatively charged SUVs coat on the surface of RIM/RIM-BP droplets. In each case, 5 μM RIM/Cy3-RIM-BP was mixed with 10 μM DiO-SUVs (A, DOPS-SUV; B, POPC-SUV; C, PIP2-SUV). Buffer condition: reaction buffer (20 mM HEPES [pH 7.5], 100 mM NaCl, 1 mM tris(2-carboxyethyl)phosphine [TCEP]) was used throughout this study unless otherwise specified. In each panel, a yellow dashed box was selected for zoomed-in analysis with a dashed line indicating the line scanning analysis of the fluorescence intensities of the SUV-coated droplet. The proteins used throughout the study were sparsely labeled with 1% of fluorophore.

(D) Statistical analysis of the coating efficiencies of RIM/RIM-BP droplets by PIP2-, DOPS-, and DOPC-SUVs. A total of 100 arbitrarily picked droplets from 10 independent images for each group were analyzed. Values were represented as mean ± SD. ****$p < 0.0001$ using one-way ANOVA with Tukey's multiple comparisons test. Statistical analysis was performed in GraphPad Prism.

(E) Representative images of FRAP analysis of the Cy3-RIM-BP signal recovery in a RIM/Cy3-RIM-BP droplet coated by DOPS-SUVs. To avoid potential signal crosstalk, only RIM-BP was labeled by Cy3. The yellow dashed box with an arrowhead indicates the droplet selected for photobleaching, and the other dashed box indicates the droplet selected as the control.

(F) Fluorescence signal recovery curves of Cy3-RIM-BP after photobleaching of RIM/RIM-BP droplets coated by PIP2-, DOPS-, and DOPC-SUVs or without SUV coating. Signals from six droplets were averaged for each type of SUVs. Data were represented as mean ± SD.

(legend continued on next page)

Please cite this article in press as: Wu et al., Vesicle Tethering on the Surface of Phase-Separated Active Zone Condensates, Molecular Cell (2020), https://doi.org/10.1016/j.molcel.2020.10.029

assembly on the surface of membranes (Wu et al., 2019). The formation of condensed RIM/RIM-BP/VGCC-CT on the surface of lipid membranes via phase separation provides an explanation to how condensed active zone protein assemblies, which are not enclosed by any physical barriers, can form at presynaptic boutons. The highly dynamic nature of the RIM/RIM-BP/VGCC-CT condensates may also explain why the dense projection structures in active zones can be observed by electron microscopy (EM) only when synapses are chemically fixed. The presence of dense RIM clusters within the active zone has also been observed in living neurons (Tang et al., 2016). Phase separation-mediated formation of condensed molecular assemblies has also been suggested to form the postsynaptic density (Zeng et al., 2016, 2018) and for α-amino-3-hydroxy-5-methyl-4-isoxazolepropionic acid receptor (AMPA) receptor synaptic clustering and transmission (Zeng et al., 2019). Formation of condensed molecular assemblies via phase separation is likely to be advantageous for synapse formation and plasticity (Chen et al., 2020; Wu et al., 2020), although such research is in its early stage.

Although tethering of SVs to release sites of presynaptic membranes requires the active zone, how SVs are physically tethered to active zones is not known. Recently, Milovanovic et al. (2018) showed that lipid vesicles can be clustered by coacervation with the synapsin condensates, providing a mechanism for maintaining large reserve pool SVs away from active zones. However, numerous EM studies have shown that tethered SVs are discretely distributed within active zone sheets and the number of tethered SVs is linearly proportional to the areas of active zone sheets (Holderith et al., 2012; Imig et al., 2014; Schikorski and Stevens, 1997; Siksou et al., 2007). In EM images of chemically fixed synapses, SVs are evenly separated by the dense projections, which are grid-like structures on active zone sheets (Bloom and Aghajanian, 1966; Gray, 1963; Limbach et al., 2011; Pfenninger et al., 1969). In addition, perturbation of synapsin affects only the reserve pool SVs, and the tethered pool remains unchanged (Pieribone et al., 1995; Rosahl et al., 1995). Conversely, disruption of active zone scaffolds impairs only the tethered pool SVs without changing the reserve pool (Acuna et al., 2016; Wang et al., 2016). Thus, tethering of SVs to the active zones is likely mediated by mechanisms that are very different from that seen in the reserve pool SV clustering by synapsin.

In this study, we demonstrate that negatively charged liposomes, as well as SVs purified from rat brains, coat on the surface of the phase-separated RIM/RIM-BP condensates. By tethering VGCC-CT to the giant unilamellar vesicle (GUV) membranes, we show that the RIM/RIM-BP condensates can bind to and cluster VGCC-CT on GUV membranes on one hand and link SUVs on the other hand, resembling active zone-mediated tethering of SVs to presynaptic membrane release sites. Remarkably, the synapsin-clustered SUV condensates and the SUV-coated RIM/RIM-BP condensates form phase-in-phase assemblies, which recapitulate coexistence of reserved and tethered pools of SVs in presynaptic boutons. The finding that the RIM/RIM-BP condensates can simultaneously link two totally different types of membrane-based cellular organelles suggests a wide range of unanticipated cellular roles of membraneless biological condensates formed by phase separation.

RESULTS

Negatively Charged SUVs Coat on the Surface of the RIM/RIM-BP Condensates

We prepared small unilamellar vesicles (SUVs) composed of 78% 1-palmitoyl-2-oleoyl-glycero-3-phosphocholine (POPC) and 20% 1,2-dioleoyl-sn-glycero-3-phospho-L-serine (DOPS) supplemented with 2% 3,3-Dioctadecyloxacarbocyanine (DiO) dye (referred to as "DOPS-SUV" hereafter) and with diameter ~30 nm to mimic SVs and studied their interaction with the RIM/RIM-BP condensates (Wu et al., 2019). The SUVs alone were homogeneously distributed in solution but became enriched on the surface of the phase-separated RIM/RIM-BP droplets (Figure 1A). We repeated the SUV coating experiment with different dyes (e.g., 1,1-Dioctadecyl-3,3,3,3-tetramethylindocarbocyanine [DiI] shown in Figure S1A) and observed the same SUV coating on the surface of the RIM/RIM-BP droplets. 3D reconstruction of SUV-coated RIM/RIM-BP droplets clearly showed that SUVs did not penetrate the RIM/RIM-BP condensates. In contrast, as it was reported earlier (Milovanovic et al., 2018), synapsin can cluster DOPS-SUVs by forming coacervated condensates (see Figure S1B). Irrelevant protein condensates, such as the PSD-95/SynGAP condensates (Zeng et al., 2016), neither clustered nor coated DOPS-SUVs (Figure S1C), suggesting that the coating of SUVs on the RIM/RIM-BP droplets is specific.

RIM is highly positively charged with an isoelectric point (pI) ~9.4. We hypothesized that the RIM/RIM-BP condensates may prefer negatively charged SUVs (e.g., DOPS-SUV). Indeed, neutral SUVs (98% POPC + 2% DiO, termed as "POPC-SUV") displayed negligible coating on the RIM/RIM-BP droplets (Figure 1B). 1,2-dioleoyl-sn-glycero-3-phospho-(1'-myo-inositol-4',5'-bisphosphate) (PI(4,5)P2) has been reported as a binding partner of RIM-C2 domains (de Jong et al., 2018). Adding 2% of PI(4,5)P2 to DOPS-SUV (i.e., 76% POPC + 20% DOPS + 2% PI(4,5)P2 + 2% DiO, termed "PIP2-SUV") increased the coating of SUVs on the RIM/RIM-BP droplets (Figure 1C; quantified in Figure 1D). The concentrations of RIM/RIM-BP in the condensates, with or without SUV coating, did not change (Figures S1D and S1E).

We showed earlier on that RIM alone and some of its fragments together with RIM-BP can undergo phase separation (Wu et al., 2019). We tested these fragments and found that condensates formed by the full-length RIM or RIM-PAS/RIM-BP could be coated by DOPS-SUV (Figures S1F and S1G). Further truncations of RIM eliminated the DOPS-SUV coating on the

(G) Fusion of the DOPS-SUV-coated RIM/RIM-BP droplets. The RIM/RIM-BP droplets were indicated by Cy3-RIM-BP, and DOPS-SUVs were labeled by DiO. Two droplets next to each other (indicated by an arrowhead) fuse into a larger droplet over time. See also Video S1.

(H) The dispersion of the DOPS-SUV-coated RIM/RIM-BP droplets by injection of the third SH3 domain of RIM-BP to the imaging chamber. See also Video S2.

All experiments presented in this and the following figures have been repeated at least three times using different batches of prepared proteins and vesicles. See also Figures S1 and S2.

Please cite this article in press as: Wu et al., Vesicle Tethering on the Surface of Phase-Separated Active Zone Condensates, Molecular Cell (2020), https://doi.org/10.1016/j.molcel.2020.10.029

condensates (Figure S1H), in accordance with an earlier study showing the direct interaction between RIM C2 domains and negatively charged lipids (de Jong et al., 2018).

ELKS functions together with RIM in the active zone formation and functions (Held and Kaeser, 2018; Wang et al., 2016). The C-terminal PSD-95, Dlg, ZO-1 (PDZ) binding motif of ELKS1 binds to the PDZ domain of RIM (Lu et al., 2005). We purified a large fragment of ELKS1 (aa141H-660S fused to aa938P-948A; Figure S2A). This ELKS1 protein could undergo phase separation with RIM (Figure S2A), in line with an earlier study showing that ELKS1 can form condensates by itself (Sala et al., 2019). Importantly, DOPS-SUVs also coated condensates formed by the RIM and ELKS1 mixture (Figure S2B). ELKS2 shares high sequence homology and domain organization similarity with ELKS1 (Held and Kaeser, 2018), but ELKS2 is more reliably distributed in the active zone (Nyitrai et al., 2020). We showed that ELKS2 can also undergo liquid-liquid phase separation (LLPS) with RIM (Figure S2C) and mediate DOPS-SUV coating (Figure S2D). We further showed that both ELKS1 and ELKS2 can promote phase separation of RIM like RIM-BP does (Figure S2E). Thus, we do not differentiate the two isoforms of ELKS proteins in this study.

SUV-Coated RIM/RIM-BP Condensates Are Highly Dynamic

Fluorescence recovery after photobleaching (FRAP)-based assay of Cy3-labeled RIM-BP in the condensates showed that the fluorescence signals of proteins in the condensates, with or without SUV coating and with coating of SUVs containing different negatively charged lipids, were all recovered with similar kinetics and amplitudes (Figures 1E and 1F), revealing that the coating by SUVs does not "seal" the protein condensates.

The dynamic properties of both proteins and SUVs in the SUV-coated RIM/RIM-BP droplets were further illustrated by fusion of the contacting droplets into larger ones accompanied by coalescence of the coated SUVs on the surface of the larger protein droplets (Figure 1G; Video S1). Under the fluorescence microscope, the fusion process of the coated SUVs is analogous to fusions of membrane bilayers of two membrane-based organelles, but the coalescence of SUV coats does not involve membrane fusion and does not require extra energy input (i.e., a spontaneous process). The third SH3 domain of RIM-BP strongly binds to RIM and can disperse the RIM/RIM-BP condensates by disrupting the multivalency of the RIM/RIM-BP network (Wu et al., 2019). Injection of the SH3 domain dispersed the SUV-coated RIM/RIM-BP condensates (Figure 1H; Video S2), further indicating that proteins such as the SH3 domain can freely cross the SUV coat.

Imaging Surface Coating of SUVs on RIM/RIM-BP Condensates by EM

We used EM to directly image the SUV coating on the RIM condensates. Negative staining EM images showed that free SUVs are quite homogeneous with diameters comparable with SVs (Figure 2A). We next used cryo-EM to directly image the coating of SUVs on the RIM droplets. Each RIM and SUV mixture was deposited onto a carbon-based EM grid with sample holes. Those small RIM droplets filling part of the sample holes were selected for imaging analysis (Figures 2B–2D). Cryo-EM images revealed that DOPS-SUVs and PIP2-SUVs were massively enriched on the surface of the RIM droplets (Figures 2B and 2C; quantified in Figures 2E and 2F). In contrast, POPC-SUVs scarcely contacted the surface of RIM droplets (Figure 2D; quantified in Figures 2E and 2F). These EM images, together with the fluorescent imaging results, revealed that negatively charged SUVs coat the surface of the RIM droplets autonomously.

SVs Purified from Rat Brains Coat on the Surface of RIM/RIM-BP Condensates

We next prepared another version of SUVs mimicking the lipid compositions of real SVs: 44.7% cholesterol + 53.3% × (46% POPC + 40% DOPE + 12% DOPS + 2% PI(4,5)P2) + 2% DiO (referred to as "cholesterol-SUV" hereafter) (Takamori et al., 2006). The cholesterol-SUVs also coated the RIM/RIM-BP droplets (Figure S3A). In contrast, the EGFP-synapsin/Intersectin (ITSN) condensates (referred to as "synapsin condensates" hereafter) coacervated with cholesterol-SUVs via co-phase separation (Figure S3B).

We next purified SVs from rat brains (Takamori et al., 2006). The purified SVs are high homogeneity (Figure S3C) and free of contaminations from plasma membrane fragments, outer mitochondria membranes, or post-synaptic proteins (Figure S3D). SVs were labeled with DiO (Kiessling et al., 2013). Satisfyingly, DiO-SVs also coated the surface of the RIM/RIM-BP droplets, although DiO-SVs were prone to forming small aggregates (Figure S3E). We replaced the hydrophobic DiO with more amphiphilic DiD for SV labeling (see Materials and Methods). DiD-SVs evenly coated the RIM/RIM-BP condensates (Figure 3A). DiD alone showed no coating on or enrichment in the RIM/RIM-BP droplets (Figure S3F), indicating that the coatings of RIM/RIM-BP droplets by the dye-labeled SVs were not artifacts of the dyes used to sparsely label SVs. DiD-SVs, like negatively charged SUVs, were coacervated with synapsin condensates (Figure S3G). In addition, DiD-SVs neither coated the surface of nor coacervated with the postsynaptic density protein 95/Synaptic Ras GTPase-activating protein (PSD95/SynGAP) condensates (Figure S3H).

SVs contain high densities of proteins on their membranes, and some of these proteins can sense action potential-induced Ca^{2+} signals (Takamori et al., 2006; Wilhelm et al., 2014). Inclusion of either 1 mM Ca^{2+} or 1 mM EDTA in the assay buffer did not have an observable impact on the coating of DiD-SVs on the surface of RIM/RIM-BP droplets (Figures 3B and 3C; quantified in Figure 3F), suggesting that the coating of SVs onto the RIM/RIM-BP droplets is Ca^{2+} independent. Finally, we digested the SV proteins that are exposed to the cytoplasm with trypsin. Trypsin digestion dramatically shifted proteins on SVs to lower molecular weights (Figure 3D). The trypsin digestion was stopped by aprotinin. The trypsin-digested SVs were found to coat the RIM/RIM-BP droplets much like the undigested SVs (Figure 3E; quantified in Figure 3F), indicating that the coating of SVs to the RIM/RIM-BP condensates is primarily mediated by lipids on SVs. If the trypsin digestion of SVs was not stopped with aprotinin, mixing of the trypsin-digested SVs with the RIM/RIM-BP condensates led to elimination of RIM/RIM-BP droplets and dispersed distribution of DiD-SVs (Figure S3I), because of the digestion of RIM and RIM-BP by trypsin. Taken together, SVs purified from rat brains can also coat on the surface of the RIM/RIM-BP condensates via lipid-protein interactions.

Please cite this article in press as: Wu et al., Vesicle Tethering on the Surface of Phase-Separated Active Zone Condensates, Molecular Cell (2020), https://doi.org/10.1016/j.molcel.2020.10.029

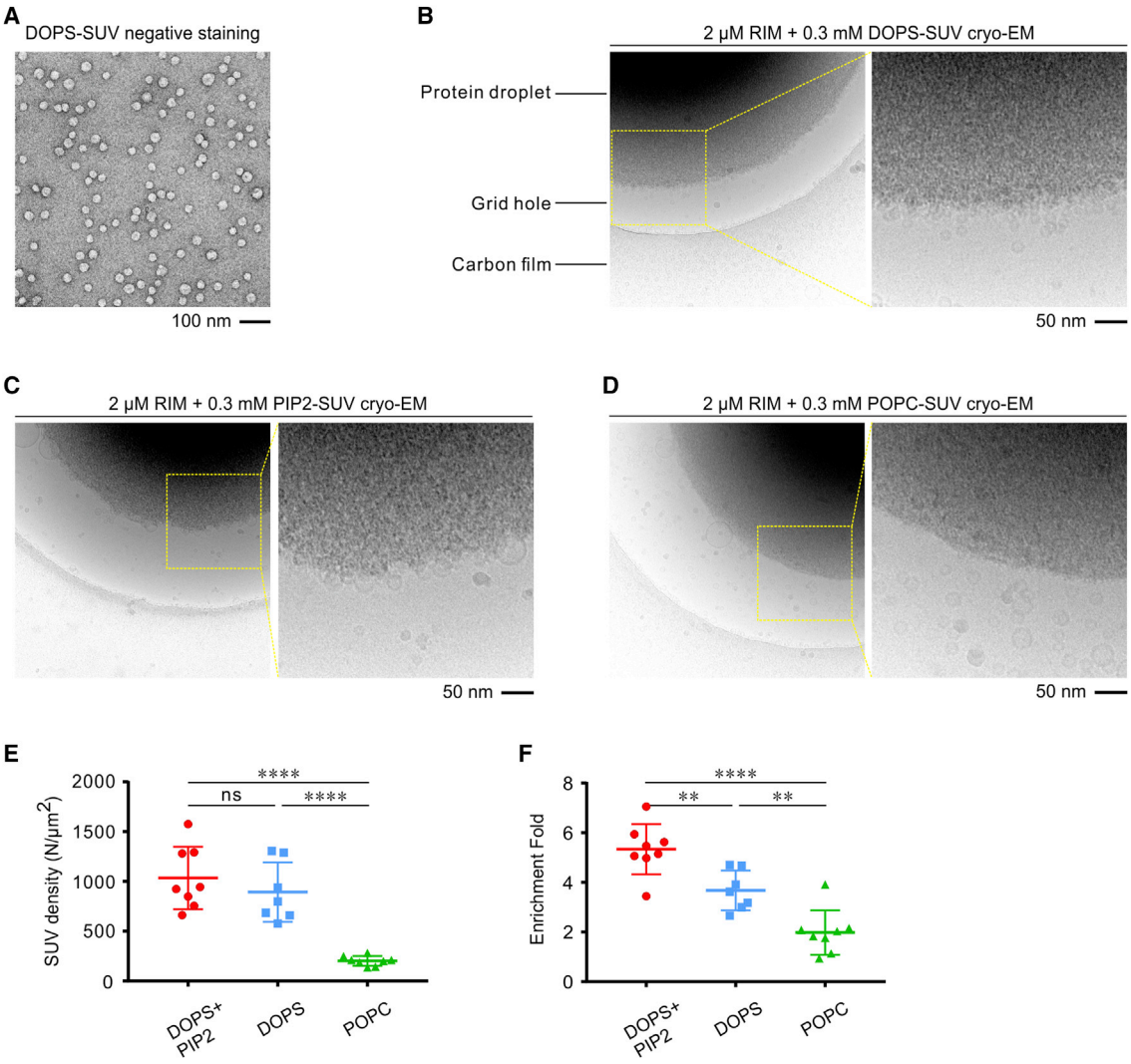

Figure 2. Imaging Surface Coating of SUVs on RIM/RIM-BP Condensates by EM

(A) An EM image of negatively stained DOPS-SUVs (15 ng/μL).

(B) Cryo-EM image of a mixture of 225 ng/μL (0.3 mM) DOPS-SUVs and 300 ng/μL (2 μM) RIM. An enlarged image is to show numerous SUVs coating on the surface of the condensed RIM droplet.

(C) Cryo-EM image of a mixture of 0.3 mM PIP2-SUVs mixed with 2 μM RIM. An enlarged image is to show numerous PIP2-SUVs coating on the surface of the condensed RIM droplet.

(D) Cryo-EM image of a mixture of 0.3 mM POPC-SUVs mixed with 2 μM RIM. An enlarged image is to show that no obvious POPC-SUVs are coated on the surface of the protein droplet. Instead, many SUVs are observed in the dilute phase outside the protein droplet.

(E and F) Quantification and comparison of cryo-EM images of RIM droplets with different SUV coating. A total of eight images from each group were analyzed. A layer with the thickness of 40 nm (a value comparable with the diameter of the SUVs) from the edge of the protein droplets was defined as the condensate surface (S1) and the surrounding area within the EM grid hole as the dilute solution area (S2). The number of SUVs in the surface area (N1) and in the solution area (N2) was counted. Two parameters were used to measure the coating efficiency. (E) SUV density on the surface of protein droplets, which is defined as N1/S1. (F) SUV enrichment fold, which is defined as (N1/S1)/((N1+N2)/(S1+S2)). ns, not significant, $p > 0.05$; **$p < 0.005$; ****$p < 0.0001$ using one-way ANOVA with Tukey's multiple comparisons test. Statistical analysis was performed in GraphPad Prism.

Tethering of SUVs on the Surface of RIM/RIM-BP Condensates Attached to the Ca^{2+}-Channel-Containing Membranes

Because active zones are attached to the presynaptic plasma membranes, we next asked whether SUVs coating could occur when the RIM/RIM-BP condensates were attached to membranes. GUVs prepared for this study are at ~10 μm in diameter. Compared with the SUVs or SVs that are within ~40 nm in diameter, the membrane curvature of GUVs is negligible (Figure 4A). Hence we used the membranes of GUVs to mimic the presynaptic plasma membranes. GUVs were labeled by 2% Cy5-Phosphatidylethanolamine (PE) (Figure 4B). We doped the GUV membrane with 5% 1,2-dioleoyl-sn-glycero-3-[(N-(5-amino-1-carboxypentyl)iminodiacetic acid)succinyl] (DGS-Ni^{2+}-NTA),

Please cite this article in press as: Wu et al., Vesicle Tethering on the Surface of Phase-Separated Active Zone Condensates, Molecular Cell (2020), https://doi.org/10.1016/j.molcel.2020.10.029

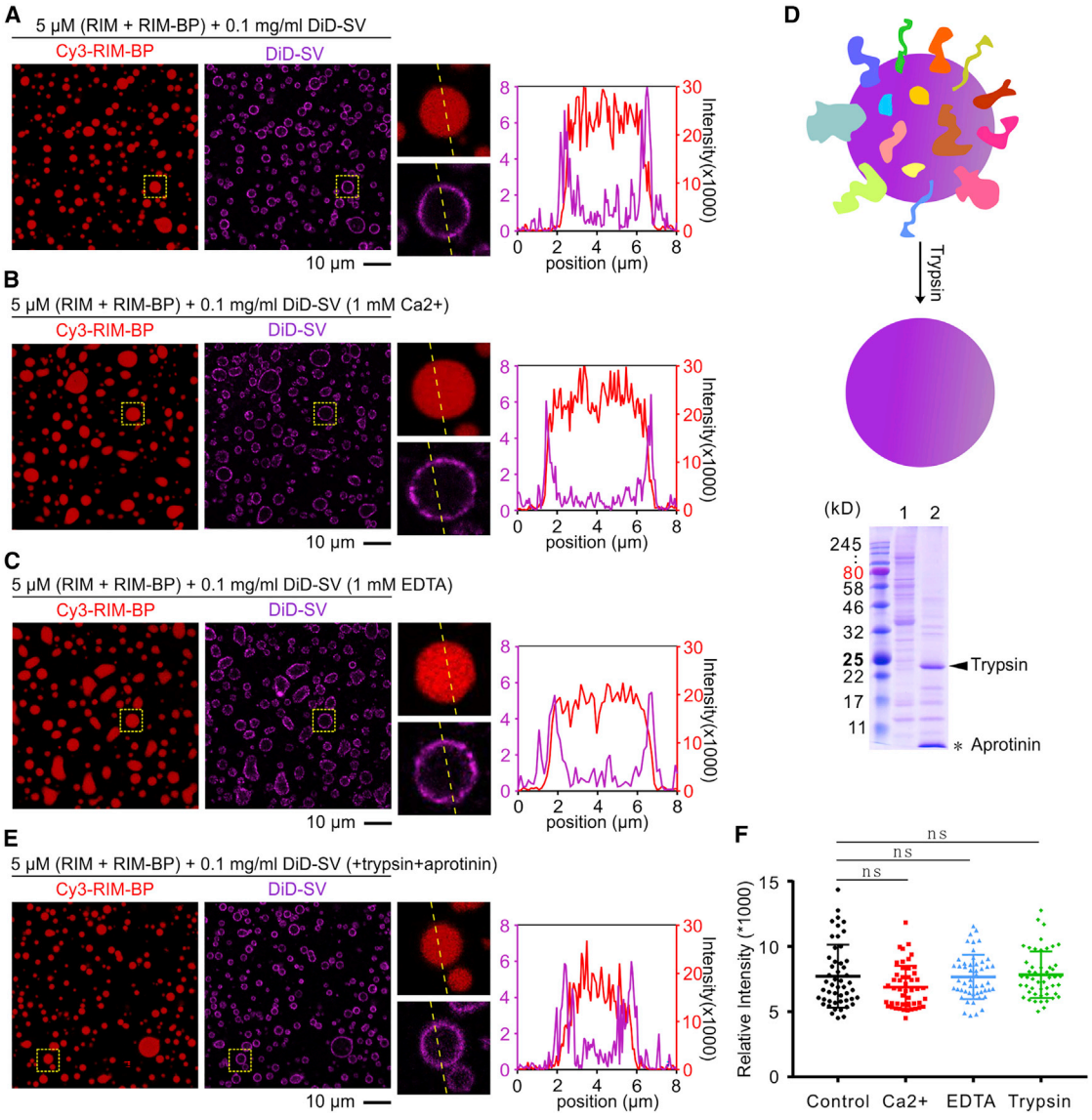

Figure 3. SVs Purified from Rat Brains Coat on the Surface of RIM/RIM-BP Condensates

(A) SVs coat the surface of the RIM/RIM-BP droplets. A yellow dashed box was selected for zoomed-in analysis, with a dashed line indicating the line scanning analysis of the fluorescence intensities of the coated droplet. Buffer condition: SV buffer (20 mM HEPES [pH 7.5], 100 mM KCl). All experiments with SVs used SV buffer unless otherwise specified.

(B and C) SVs coat the surface of the RIM/RIM-BP droplets with SV buffer containing 1 mM Ca^{2+} (B) or 1 mM EDTA (C). The assay condition is the same as in (A).

(D) Upper panel: a schematic illustration showing trypsin digestion of proteins on the surface of an SV. Lower panel: a representative SDS-PAGE of SVs before (lane 1) and after (lane 2) trypsin digestion. The black arrowhead indicates the added trypsin; the asterisk indicates the added aprotinin.

(E) Coating of the RIM/Cy3-RIM-BP condensates by trypsin-digested SVs. SVs were digested with trypsin (0.025 mg/mL, final concentration), and the digestion reaction was stopped by addition of aprotinin (0.025 mg/mL, final concentration).

(F) Quantification and comparison of relative fluorescence intensities of SVs on the surface of RIM/RIM-BP droplets with buffer containing Ca^{2+}, EDTA, or trypsin (with addition of aprotinin at the end of SV protein digestion) and the control group. A total of 50 arbitrarily picked droplets from five independent images for each group were analyzed. Values were represented as mean ± SD. Statistical analysis was performed in GraphPad Prism. ns, nonsignificant using one-way ANOVA with Dunnett's multiple comparisons test.

See also Figure S3.

which was used to capture His_6-tagged VGCC-CT (Figure 4B; Wu et al., 2019). Addition of RIM and RIM-BP to the GUV-containing solution led to the phase separation of RIM and RIM-BP together with concentration of VGCC-CT on the surface of GUVs (Figure 4C; Video S3). Phase separation also occurred in the solution as expected (the bright spherical droplets containing RIM, RIM-BP, and VGCC-CT in solution that are not attached to the GUVs in Figure 4C; Wu et al., 2019). We repeated this

Please cite this article in press as: Wu et al., Vesicle Tethering on the Surface of Phase-Separated Active Zone Condensates, Molecular Cell (2020), https://doi.org/10.1016/j.molcel.2020.10.029

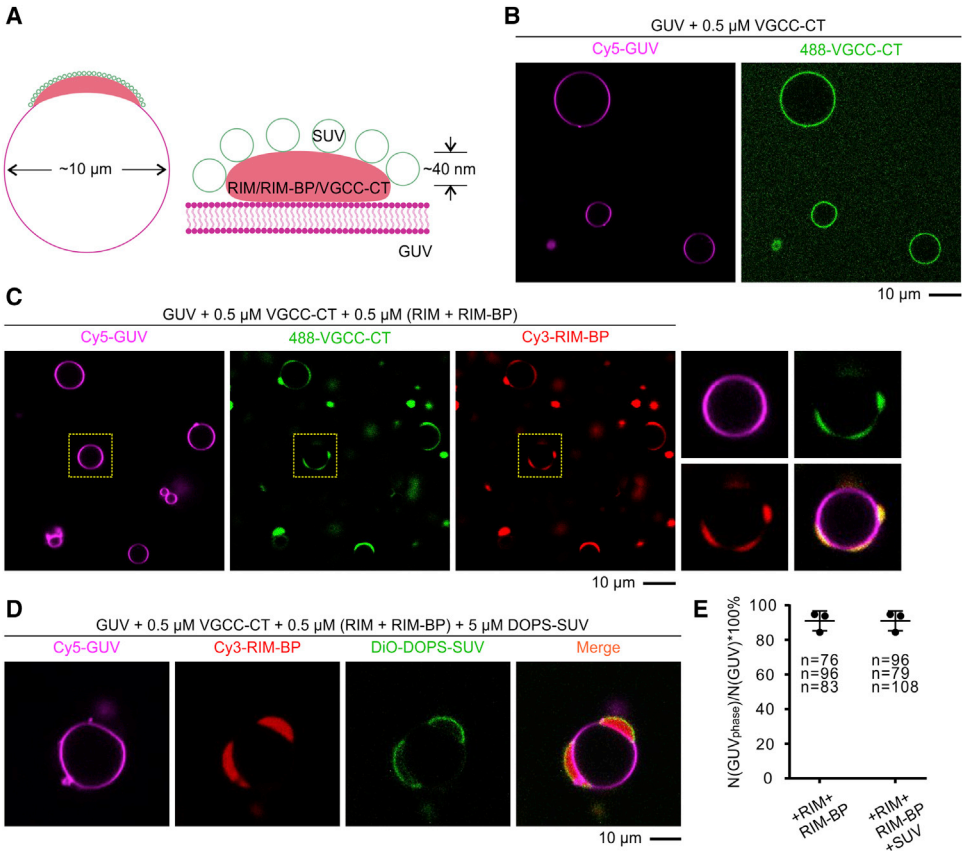

Figure 4. Tethering of SUVs on the Surface of RIM/RIM-BP Condensates Attached to Ca^{2+} Channel-Tethered GUV Membranes

(A) A schematic illustration showing that a RIM/RIM-BP condensate attaches to GUV membrane with its one face and interacts with SUVs with the other surface. Considering the relative sizes of a typical GUV (~10 μm) and an SUV (~30 nm), the GUV membrane can be regarded as flat to mimic the plasma membrane. His_6-tagged VGCC-CT was tethered to the GUV surface via His_6-NTA, and RIM/RIM-BP could undergo phase separation on the surface of GUV using VGCC-CT as a tether. SUVs can further coat the surface of the RIM/RIM-BP/VGCC-CT condensate.

(B) Incubation of 0.5 μM iFluor 488-VGCC-CT with Cy5-GUV showing tethering of VGCC-CT to the GUVs. Every GUV imaged was tethered by VGCC-CT. Buffer condition: PBS. All the following experiments with GUV used PBS unless otherwise specified.

(C) Addition of 0.5 μM RIM/Cy3-RIM-BP to the VGCC-CT tethered GUVs led to phase separation of RIM/RIM-BP/VGCC-CT on the surface of GUVs. One GUV highlighted with a dashed box was selected for zoomed-in analysis. See also Video S3.

(D) Addition of DiO-DOPS-SUVs to the RIM/RIM-BP/VGCC-CT/GUV system as described in (C) led to DOPS-SUVs coating on the outer surface of the RIM/RIM-BP droplet attached to the GUV membrane. See also Video S4.

(E) Quantification of percentage of GUVs with RIM/RIM-BP condensates attached to the GUVs. Data were derived from three different batches of experiments. "n" represents number of GUVs that were randomly chosen for analysis in each batch (i.e., 76, 96, and 83 GUVs were selected from each batch; left column). The same quantification method was used for (D) to show the percentage of GUVs with SUV-coated RIM/RIM-BP condensates attached to the GUVs (right column). See also Figure S4.

reconstitution assay in three different batches of experiments and calculated the percentage of GUVs with RIM/RIM-BP/VGCC-CT condensates attached. The quantification data showed that RIM/RIM-BP/VGCC-CT undergo phase separation on the vast majority of the GUVs (Figure 4E, left).

We then added 5 μM DOPS-SUVs to the GUV system containing RIM, RIM-BP, and VGCC-CT. Strikingly, the SUVs were tethered to the solvent-exposed side of the RIM/RIM-BP/VGCC-CT condensates adhered to the surface of GUVs (Figure 4D; Video S4; quantified in Figure 4E, right), forming an assembly reminiscent of SVs tethered to the RIM/RIM-BP-containing active zone attached to the presynaptic plasma membranes. FRAP assay showed that proteins (e.g., Cy3-labeled RIM-BP) in the system shown in Figure 4D remain dynamic (Figure S4A).

VGCCs were recently reported to be dispensable for active zone assembly (Held et al., 2020), in line with our previous *in vitro* finding showing that RIM and RIM-BP undergo LLPS without requiring VGCC-CT (Wu et al., 2019). We examined the phase separation and SUV coating of RIM and RIM-BP on the GUV in the absence of VGCC-CT. Because RIM/RIM-BP are associated with presynaptic plasma membranes, PIP2 was used to test whether this negatively charged lipid can anchor the RIM/RIM-BP droplets to GUVs. PIP2-containing GUV (96% POPC + 2% PI(4,5)P2 + 2% Cy5-PE) was prepared to mimic the VGCC-CT free plasma membrane. Indeed, the RIM and

Please cite this article in press as: Wu et al., Vesicle Tethering on the Surface of Phase-Separated Active Zone Condensates, Molecular Cell (2020), https://doi.org/10.1016/j.molcel.2020.10.029

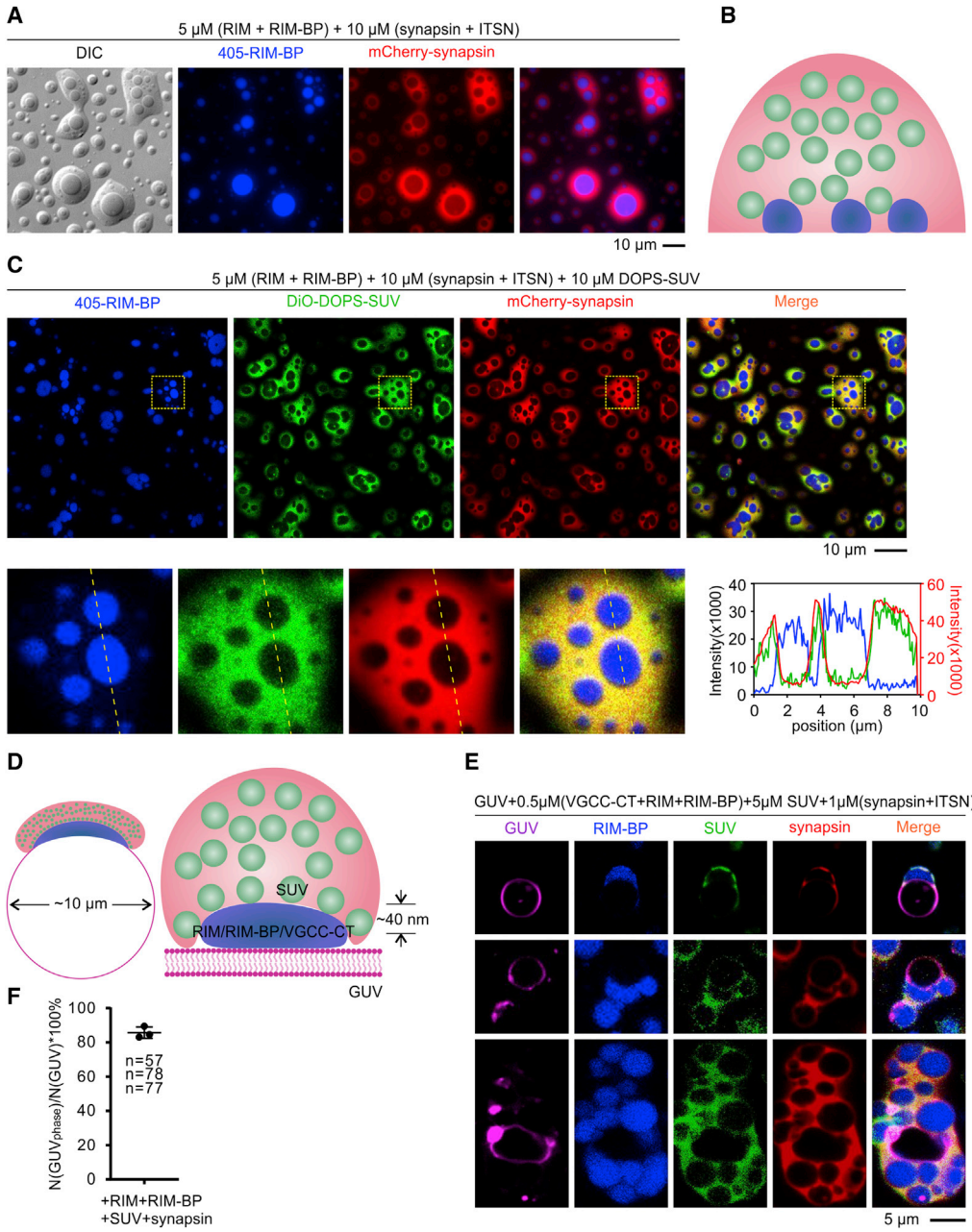

Figure 5. Synapsin Condensates and RIM/RIM-BP Condensates Organize Reserve and Tethered Pools of SVs into Distinct Subcompartments

(A) Differential interference contrast (DIC) and fluorescent images of RIM/RIM-BP (5 μM) mixed with mCherry-synapsin/ITSN (10 μM) showing encapsulation of the RIM/RIM-BP droplets by the synapsin condensates. The encapsulation is very robust; every RIM/RIM-BP droplet imaged was encapsulated by the synapsin/ITSN condensates in many batches ($n > 5$) of experiments performed. Buffer condition: reaction buffer supplemented with 3% PEG8000 to trigger synapsin phase separation (Milovanovic et al., 2018).

(B) A schematic diagram showing two pools of SUVs. The majority of SUVs are clustered by synapsin via co-phase separation. A small population of SUVs coat on the surface of RIM-RIM-BP droplets, which are encapsulated by the SUV/synapsin condensates.

(C) DOPS-SUVs are clustered by the synapsin condensates and coated on the surface of RIM/RIM-BP droplets. The DOPS-SUV-coated RIM/RIM-BP droplets are encapsulated by the SUV/synapsin condensates. Again, every RIM/RIM-BP droplet imaged was encapsulated by the SUV/synapsin condensates in multiple ($n > 5$) independent batches of experiments. In this assay, RIM/iFluor 405-RIM-BP (5 μM), mCherry-synapsin/ITSN (10 μM), and DiO-DOPS-SUV (10 μM) were mixed, and the phase-in-phase assembly immediately formed upon mixing. One region highlighted with a dashed box was magnified for further analysis. Line scanning analysis is used to show the distribution profiles of different labeled components in this phase-in-phase system. Buffer condition: reaction buffer supplemented with 3% PEG8000.

(legend continued on next page)

Please cite this article in press as: Wu et al., Vesicle Tethering on the Surface of Phase-Separated Active Zone Condensates, Molecular Cell (2020), https://doi.org/10.1016/j.molcel.2020.10.029

RIM-BP mixture phase separated on PIP2-containing GUVs, and SUVs coated the outer surface of the RIM/RIM-BP droplets (Figure S4B). As a control, VGCC-CT alone cannot mediate the association between SUVs and GUVs (Figure S4C).

Synapsin Condensates and RIM/RIM-BP Condensates Organize Reserve and Tethered Pools of SVs into Distinct Subcompartments

The reserve pool and readily releasable pool of SVs are functionally distinct, but each lacks specific morphological features or explicit molecular markers (Alabi and Tsien, 2012). A central unaddressed question is how the two pools of SVs are differentially separated but at the same time capable of exchanging with each other. Because SUVs and SVs coat on the surface of the RIM/RIM-BP condensates but coacervate with the synapsin condensates (Figures 1 and 3), we asked what would occur if the RIM/RIM-BP condensates and the synapsin condensates were mixed together in a way analogous to their co-existence in presynaptic terminal boutons. Surprisingly, the synapsin condensates and the RIM/RIM-BP condensates were immiscible, and the synapsin condensates always encapsulate the RIM/RIM-BP droplets (Figure 5A), suggesting that synapsin and RIM/RIM-BP can form two distinct phases in terminal boutons: one for clustering reserve pool SVs and the other for tethering readily releasable SVs (Figure 5B). Similarly, the RIM/ELKS condensates were also enveloped by the synapsin condensates (Figure S5A). Intriguingly, a synapsin fragment containing the dimerization domain C and the intrinsic disordered domain D (termed "synapsin-CD"), which is competent for phase separation and for clustering SVs, could no longer encapsulate with the RIM/RIM-BP droplets but instead coacervated with the RIM/RIM-BP droplets (Figure S5B), indicating that the less characterized short and unstructured regions outside the CD part of synapsin are critical for separating the synapsin condensates from the RIM/RIM-BP condensates. The encapsulation of the RIM/RIM-BP droplets by the synapsin condensates was independent of the order of mixing of the protein components—for example, addition of RIM and RIM-BP to a solution containing preformed synapsin condensates, the RIM/RIM-BP condensates nucleated and matured inside the synapsin condensates. The RIM/RIM-BP condensates that formed outside the synapsin condensates also eventually entered the synapsin condensates (Figure S5C; Video S5).

We then added DOPS-SUVs to the mixed-phase system composed of the synapsin condensates and the RIM/RIM-BP condensates. Remarkably, SUVs coacervated with and were consequently concentrated by the synapsin phase. These synapsin/SUV condensates further encapsulated the RIM/RIM-BP droplets (Figure 5C). SUVs coated the surface of the RIM/RIM-BP droplets but did not enter the droplets (Figure 5C). Both RIM-BP and synapsin were dynamic as probed by FRAP assays, although RIM-BP in the inner core of the assembly appeared to recover with a lower speed (Figures S6A and S6B). In addition, the injection of the third SH3 domain of RIM-BP resulted in gradual dispersion of the RIM/RIM-BP droplets (Figure S6C), further confirming the mobility of RIM/RIM-BP even when enveloped by synapsin/SUV co-condensates. Taking the vastly higher concentration of synapsin than those of RIM and RIM-BP into consideration, most SVs in a presynaptic bouton would be clustered by the synapsin condensates. Only a limited number of SVs are coated on the active zone surface because of the small active zone surface area. Because the synapsin/SV condensates encapsulate the RIM/RIM-BP/SV droplets, SVs in the two phases are free to exchange (Figure 5D).

Finally, we attempted to reconstitute the synapsin/SUV and RIM/RIM-BP/SUV condensates with VGCC-CT-tethered GUVs, aiming to generate an *in vitro* model system capturing the two pools of SVs in presynaptic boutons (Figure 5D). In solution containing VGCC-CT-tethered GUVs, we sequentially added the RIM/RIM-BP condensates, the synapsin condensates, and DOPS-SUVs. We observed that the RIM/RIM-BP droplets were attached to the GUV surface on one face and coated by SUVs on the other face. Such SUV-coated RIB/RIM-BP droplets were further surrounded by synapsin/SUV co-condensates (Figure 5E; Video S6; quantified in Figure 5F). Thus, we have reconstituted a minimalistic version of presynaptic bouton containing reserve and tethered pools of SVs. Again, VGCC-CT here served as an anchor between RIM/RIM-BP and GUVs. When VGCC-CT on GUVs was replaced by PIP2, the presynaptic bouton-like multiphase assembly was also formed (Figure S6D).

DISCUSSION

Tethered SVs are typically defined by their physical distance (~30 nm or less) to the presynaptic plasma membranes (Imig et al., 2014; Verhage and Sørensen, 2008). Decades of past research have identified molecules, including RIM, RIM-BP, ELKS, and Munc13, that are critical for SVs to tether and dock to presynaptic membranes (Biederer et al., 2017; Südhof, 2012). However, how SVs are retained at the active zone remains elusive. Here we discover that SVs coat on the surface of condensed droplets formed by the active zone proteins, including RIM, RIM-BP, and ELKS, via phase separation. This finding may explain several observations made in past decades of studies. First, the number of tethered SVs is proportional to the surface area of the active zone. Second, SVs coated on the

(D) A schematic diagram showing the experimental setup to capture the reserve pool and tethered pool of vesicles by the synapsin and RIM/RIM-BP condensates on the surface of GUV membrane.

(E) Realization of tethering of SUV-coated RIM/RIM-BP droplets on GUV membranes and subsequent coating of the SUV/synapsin condensates onto the solvent-exposed surface of the RIM/RIM-BP droplets. In this assay, RIM/RIM-BP (0.5 μM), mCherry-synapsin/ITSN (1 μM), and DiO-DOPS-SUV (5 μM) were added to a solution containing VGCC-CT (0.5 μM) tethered Cy5-GUVs. Three representative sample images are presented. Buffer condition: PBS supplemented with 2% PEG8000 to minimize the impact of PEG8000 on GUV stability. See also Video S6.

(F) Percentage of GUVs with RIM/RIM-BP condensates attached to the GUVs. Data were derived from three different batches of experiments. "n" represents number of GUVs randomly chosen for analysis in each batch of the experiments.

See also Figures S5 and S6.

Please cite this article in press as: Wu et al., Vesicle Tethering on the Surface of Phase-Separated Active Zone Condensates, Molecular Cell (2020), https://doi.org/10.1016/j.molcel.2020.10.029

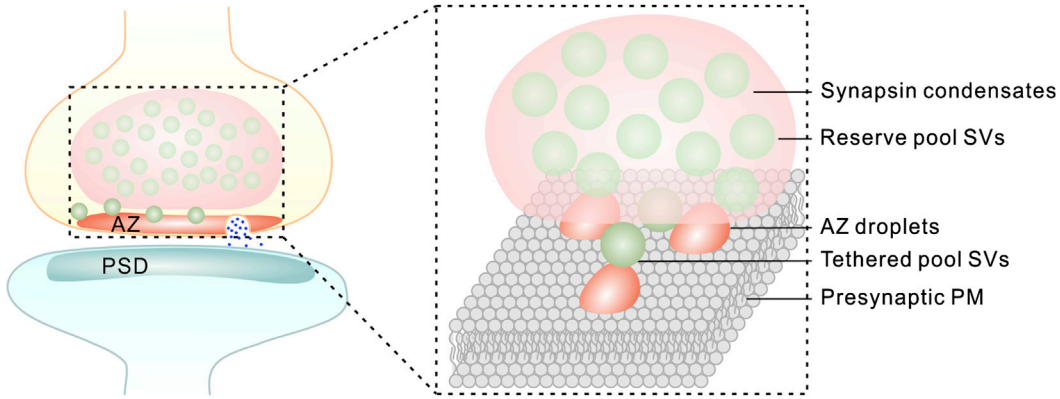

Figure 6. A Model of SV Pools Organized by Distinct Protein Condensates

Synapsin condensates and RIM/RIM-BP droplets are coexisting in a presynaptic bouton. SVs are divided into two groups by the protein condensates, with one group clustered by and coacervated with synapsin condensates, and the other one tethered to the surface of RIM/RIM-BP droplets, reminiscent of the reserve pool and tethered pool of SVs in synapses. AZ, active zone; PM, plasma membrane; PSD, post-synaptic density.

surface of RIM/RIM-BP condensates are highly dynamic but are very close to both fusion machineries and presynaptic plasma membranes; thus, such active zone tethered SVs are primed for rapid fusion. Third, the RIM/RIM-BP condensates can cluster Ca^{2+} channels on the membranes. The direct coating of SVs on the surface of the RIM/RIM-BP droplets can physically link clustered Ca^{2+} channels with SVs for Ca^{2+}-regulated fusion reactions. Fourth, formation of the RIM/RIM-BP condensates can greatly enhance the weak interaction between RIM/RIM-BP and negatively charged lipids on SVs, and thus allow stable interaction between the active zone molecular assembly and SVs. Fifth, the binding of SVs to the liquid-like active zone may shape the active zone into grid-like structures observed by EM under chemical fixing conditions. The condensed droplets formed by proteins, including RIM, RIM-BP, and ELKS, are highly dense but still very dynamic. Chemical fixation may capture such dynamic but dense assemblies referred to as dense projections. The coating of SVs on the surfaces of active zones likely involves proteins in addition to RIM, RIM-BP, and ELKS studied here. Proteins such as Munc13, Munc18, Liprin, Piccolo, Bassoon, SNAREs, the Rab family small GTPases, synaptotagmins, and so on can modulate SV docking and priming (Binotti et al., 2016; Imig et al., 2014; Kaeser and Regehr, 2017; Limbach et al., 2011; Südhof, 2012). These proteins may also participate in the regulation of active zone assembly and SVs coating. It is noted that the SV-coated RIM/RIM-BP condensates are not physically insulated by SVs. Proteins can readily enter in or escape from the SV-coated active zone protein condensates. Thus, such SV-coated active zone protein condensates can connect with molecular components both near and distal to the presynaptic membranes.

Another major finding of this study is that interactions of SVs with different protein condensates formed via phase separation can be radically different. SVs co-phase separate with synapsin, leading to clustering and concentration of SVs (Figure S3G; Milovanovic et al., 2018; Pechstein et al., 2020). Given that synapsin is massively concentrated in presynaptic boutons (Wilhelm et al., 2014), the protein is ideally suited for maintaining the vast majority of SVs as the reserve pool. Strikingly, SVs do not enter the condensed phase formed by the active zone proteins, but instead coat on the surface of the condensates. Remarkably, the synapsin/SUV condensates encapsulate the SUV-coated RIM/RIM-BP droplets when the two phase-separated condensates are mixed (Figure 5), suggesting that the synapsin-clustered reserve SV pool can coexist with the active zone-tethered SVs, and the two pools of SVs can exchange with each other. Finally, we have been able to reconstitute a minimalistic presynaptic bouton-like structure, in which the active zone-coated vesicles are attached to the presynaptic plasma membrane and the synapsin-clustered reserve pool SV condensates are situated more distal to the presynaptic plasma membrane but directly interact with the active zone condensates (Figures 5 and 6). This reconstituted system recapitulates the basic features of the SV clustering and tethering in presynaptic boutons. In real synapses, the presynaptic plasma membranes together with various membrane proteins likely serve as the starting layer structure to organize the subsequent active zone layer, tethered SVs, and synapsin-clustered reserve pool SVs, forming the elaborate and polarized multiphase organizations. It should be noted that the scale/size of the reconstituted, presynaptic bouton-like assemblies here is much larger than the sizes of real presynaptic boutons. The awkward size of presynaptic boutons has presented challenges to investigate whether the layered structures observed in EM studies are indeed formed via the multiphase organization seen in this *in vitro* study. New technologies will need to be developed to answer this question in the future.

In a broader cell biology context, distinct mode of interactions between membraneless organelles and various membrane demarcated organelles, similar to what is observed in this study, may be broadly adopted by cells to modulate processes such as organelle biogenesis, vesicle formation and trafficking, autophagy, and membrane-associated signaling assembly formation (Fujioka et al., 2020; Liao et al., 2019; Ma and Mayr, 2018; Zhao and Zhang, 2020).

Please cite this article in press as: Wu et al., Vesicle Tethering on the Surface of Phase-Separated Active Zone Condensates, Molecular Cell (2020), https://doi.org/10.1016/j.molcel.2020.10.029

STAR★METHODS

Detailed methods are provided in the online version of this paper and include the following:

- KEY RESOURCES TABLE
- RESOURCE AVAILABILITY
  - Lead contact
  - Materials availability
  - Data and code availability
- EXPERIMENTAL MODEL AND SUBJECT DETAILS
  - Bacterial strain
  - Cell line
- METHOD DETAILS
  - Genes and constructs
  - Protein expression and purification
  - Sortase-mediated protein ligation
  - Synapsin full-length expression and purification
  - Protein labeling with fluorophore
  - Small Uni-lamellar Vesicle (SUV) preparation
  - Imaging
  - SUV coating efficiency and corresponding protein intensity comparison
  - Sedimentation assay
  - Fluorescence recovery after photobleaching (FRAP) assay
  - Negative staining
  - Cryo-EM imaging
  - Synaptic Vesicle (SV) purification
  - SV characterization
  - Labeling SVs with fluorescent dyes
  - Trypsin digestion of SVs
  - Giant Uni-lamellar Vesicle (GUV) preparation and imaging
- QUANTIFICATION AND STATISTICAL ANALYSIS

SUPPLEMENTAL INFORMATION

Supplemental Information can be found online at https://doi.org/10.1016/j.molcel.2020.10.029.

ACKNOWLEDGMENTS

We thank Dr. Cong Ma from Huazhong University of Science and Technology for assistance in SUV preparation, Dr. Xueming Li from Tsinghua University for discussions in EM experiments, and members of the Zhang lab for stimulating discussions. This work was supported by grants from Research Grant Council of Hong Kong (16101419, AoE-M09-12, and C6004-17G), a grant from the Minister of Science and Technology of China (2019YFA0508402 to M.Z.), an ERC Advanced Grant (SVNeuroTrans; to M.G. and R.J.), and a CAPES-Humboldt fellowship (CAPES, 99999.002062/2014-03 to M.G.). M.Z. is a Kerry Holdings Professor of Science and a Senior Fellow of IAS at HKUST. The Biological Cryo-EM Center at HKUST is supported by a donation from the Lo Kwee Seong Foundation.

AUTHOR CONTRIBUTIONS

X.W., M.G., J.Z., and S.Z. performed experiments. X.W., M.G., J.Z., R.J., and M.Z. analyzed the data. X.W. and M.Z. designed research. X.W. and M.Z. drafted the manuscript, and all authors commented on the paper. M.Z. coordinated the project.

DECLARATION OF INTERESTS

The authors declare no competing interests.

Received: June 25, 2020
Revised: September 15, 2020
Accepted: October 16, 2020
Published: November 16, 2020

REFERENCES

Ackermann, F., Waites, C.L., and Garner, C.C. (2015). Presynaptic active zones in invertebrates and vertebrates. EMBO Rep. *16*, 923–938.

Acuna, C., Liu, X., and Südhof, T.C. (2016). How to Make an Active Zone: Unexpected Universal Functional Redundancy between RIMs and RIM-BPs. Neuron *91*, 792–807.

Alabi, A.A., and Tsien, R.W. (2012). Synaptic vesicle pools and dynamics. Cold Spring Harb. Perspect. Biol. *4*, a013680.

Biederer, T., Kaeser, P.S., and Blanpied, T.A. (2017). Transcellular Nanoalignment of Synaptic Function. Neuron *96*, 680–696.

Binotti, B., Jahn, R., and Chua, J.J. (2016). Functions of Rab Proteins at Presynaptic Sites. Cells *5*, 7.

Bloom, F.E., and Aghajanian, G.K. (1966). Cytochemistry of synapses: selective staining for electron microscopy. Science *154*, 1575–1577.

Chen, J., Billings, S.E., and Nishimune, H. (2011). Calcium channels link the muscle-derived synapse organizer laminin β2 to Bassoon and CAST/Erc2 to organize presynaptic active zones. J. Neurosci. *31*, 512–525.

Chen, X., Wu, X., Wu, H., and Zhang, M. (2020). Phase separation at the synapse. Nat. Neurosci. *23*, 301–310.

Dani, A., Huang, B., Bergan, J., Dulac, C., and Zhuang, X. (2010). Superresolution imaging of chemical synapses in the brain. Neuron *68*, 843–856.

de Jong, A.P.H., Roggero, C.M., Ho, M.R., Wong, M.Y., Brautigam, C.A., Rizo, J., and Kaeser, P.S. (2018). RIM C_2B Domains Target Presynaptic Active Zone Functions to PIP_2-Containing Membranes. Neuron *98*, 335–349.e7.

Emperador-Melero, J., and Kaeser, P.S. (2020). Assembly of the presynaptic active zone. Curr. Opin. Neurobiol. *63*, 95–103.

Fujioka, Y., Alam, J.M., Noshiro, D., Mouri, K., Ando, T., Okada, Y., May, A.I., Knorr, R.L., Suzuki, K., Ohsumi, Y., and Noda, N.N. (2020). Phase separation organizes the site of autophagosome formation. Nature *578*, 301–305.

Glebov, O.O., Jackson, R.E., Winterflood, C.M., Owen, D.M., Barker, E.A., Doherty, P., Ewers, H., and Burrone, J. (2017). Nanoscale Structural Plasticity of the Active Zone Matrix Modulates Presynaptic Function. Cell Rep. *18*, 2715–2728.

Gray, E.G. (1963). Electron microscopy of presynaptic organelles of the spinal cord. J. Anat. *97*, 101–106.

Han, Y., Kaeser, P.S., Südhof, T.C., and Schneggenburger, R. (2011). RIM determines Ca^{2}+ channel density and vesicle docking at the presynaptic active zone. Neuron *69*, 304–316.

Haucke, V., Neher, E., and Sigrist, S.J. (2011). Protein scaffolds in the coupling of synaptic exocytosis and endocytosis. Nat. Rev. Neurosci. *12*, 127–138.

Held, R.G., and Kaeser, P.S. (2018). ELKS active zone proteins as multitasking scaffolds for secretion. Open Biol. *8*, 170258.

Held, R.G., Liu, C., Ma, K., Ramsey, A.M., Tarr, T.B., De Nola, G., Wang, S.S.H., Wang, J., van den Maagdenberg, A.M.J.M., Schneider, T., et al. (2020). Synapse and Active Zone Assembly in the Absence of Presynaptic Ca^{2+} Channels and Ca^{2+} Entry. Neuron *107*, 667–683.e9.

Holderith, N., Lorincz, A., Katona, G., Rózsa, B., Kulik, A., Watanabe, M., and Nusser, Z. (2012). Release probability of hippocampal glutamatergic terminals scales with the size of the active zone. Nat. Neurosci. *15*, 988–997.

Imig, C., Min, S.W., Krinner, S., Arancillo, M., Rosenmund, C., Südhof, T.C., Rhee, J., Brose, N., and Cooper, B.H. (2014). The morphological and

molecular nature of synaptic vesicle priming at presynaptic active zones. Neuron *84*, 416–431.

Jahn, R., and Fasshauer, D. (2012). Molecular machines governing exocytosis of synaptic vesicles. Nature *490*, 201–207.

Kaeser, P.S., and Regehr, W.G. (2017). The readily releasable pool of synaptic vesicles. Curr. Opin. Neurobiol. *43*, 63–70.

Kaeser, P.S., Deng, L., Wang, Y., Dulubova, I., Liu, X., Rizo, J., and Südhof, T.C. (2011). RIM proteins tether Ca2+ channels to presynaptic active zones via a direct PDZ-domain interaction. Cell *144*, 282–295.

Kiessling, V., Ahmed, S., Domanska, M.K., Holt, M.G., Jahn, R., and Tamm, L.K. (2013). Rapid fusion of synaptic vesicles with reconstituted target SNARE membranes. Biophys. J. *104*, 1950–1958.

Kittel, R.J., Wichmann, C., Rasse, T.M., Fouquet, W., Schmidt, M., Schmid, A., Wagh, D.A., Pawlu, C., Kellner, R.R., Willig, K.I., et al. (2006). Bruchpilot promotes active zone assembly, Ca2+ channel clustering, and vesicle release. Science *312*, 1051–1054.

Liao, Y.C., Fernandopulle, M.S., Wang, G., Choi, H., Hao, L., Drerup, C.M., Patel, R., Qamar, S., Nixon-Abell, J., Shen, Y., et al. (2019). RNA Granules Hitchhike on Lysosomes for Long-Distance Transport, Using Annexin A11 as a Molecular Tether. Cell *179*, 147–164.e20.

Limbach, C., Laue, M.M., Wang, X., Hu, B., Thiede, N., Hultqvist, G., and Kilimann, M.W. (2011). Molecular in situ topology of Aczonin/Piccolo and associated proteins at the mammalian neurotransmitter release site. Proc. Natl. Acad. Sci. USA *108*, E392–E401.

Liu, K.S., Siebert, M., Mertel, S., Knoche, E., Wegener, S., Wichmann, C., Matkovic, T., Muhammad, K., Depner, H., Mettke, C., et al. (2011). RIM-binding protein, a central part of the active zone, is essential for neurotransmitter release. Science *334*, 1565–1569.

Lu, J., Li, H., Wang, Y., Südhof, T.C., and Rizo, J. (2005). Solution structure of the RIM1alpha PDZ domain in complex with an ELKS1b C-terminal peptide. J. Mol. Biol. *352*, 455–466.

Ma, W., and Mayr, C. (2018). A Membraneless Organelle Associated with the Endoplasmic Reticulum Enables 3'UTR-Mediated Protein-Protein Interactions. Cell *175*, 1492–1506.e19.

Milovanovic, D., Wu, Y., Bian, X., and De Camilli, P. (2018). A liquid phase of synapsin and lipid vesicles. Science *361*, 604–607.

Nagy, A., Baker, R.R., Morris, S.J., and Whittaker, V.P. (1976). The preparation and characterization of synaptic vesicles of high purity. Brain Res. *109*, 285–309.

Nyitrai, H., Wang, S.S.H., and Kaeser, P.S. (2020). ELKS1 Captures Rab6-Marked Vesicular Cargo in Presynaptic Nerve Terminals. Cell Rep. *31*, 107712.

Pechstein, A., Tomilin, N., Fredrich, K., Vorontsova, O., Sopova, E., Evergren, E., Haucke, V., Brodin, L., and Shupliakov, O. (2020). Vesicle clustering in a living synapse depends on a synapsin region that mediates phase separation. Cell Rep. *30*, 2594–2602.e3.

Pfenninger, K., Sandri, C., Akert, K., and Eugster, C.H. (1969). Contribution to the problem of structural organization of the presynaptic area. Brain Res. *12*, 10–18.

Pieribone, V.A., Shupliakov, O., Brodin, L., Hilfiker-Rothenfluh, S., Czernik, A.J., and Greengard, P. (1995). Distinct pools of synaptic vesicles in neurotransmitter release. Nature *375*, 493–497.

Rosahl, T.W., Spillane, D., Missler, M., Herz, J., Selig, D.K., Wolff, J.R., Hammer, R.E., Malenka, R.C., and Südhof, T.C. (1995). Essential functions of synapsins I and II in synaptic vesicle regulation. Nature *375*, 488–493.

Sakamoto, H., Ariyoshi, T., Kimpara, N., Sugao, K., Taiko, I., Takikawa, K., Asanuma, D., Namiki, S., and Hirose, K. (2018). Synaptic weight set by Munc13-1 supramolecular assemblies. Nat. Neurosci. *21*, 41–49.

Sala, K., Corbetta, A., Minici, C., Tonoli, D., Murray, D.H., Cammarota, E., Ribolla, L., Ramella, M., Fesce, R., Mazza, D., et al. (2019). The ERC1 scaffold protein implicated in cell motility drives the assembly of a liquid phase. Sci. Rep. *9*, 13530.

Schikorski, T., and Stevens, C.F. (1997). Quantitative ultrastructural analysis of hippocampal excitatory synapses. J. Neurosci. *17*, 5858–5867.

Schoch, S., and Gundelfinger, E.D. (2006). Molecular organization of the presynaptic active zone. Cell Tissue Res. *326*, 379–391.

Sclip, A., and Südhof, T.C. (2020). LAR receptor phospho-tyrosine phosphatases regulate NMDA-receptor responses. eLife *9*, e53406.

Siksou, L., Rostaing, P., Lechaire, J.P., Boudier, T., Ohtsuka, T., Fejtová, A., Kao, H.T., Greengard, P., Gundelfinger, E.D., Triller, A., and Marty, S. (2007). Three-dimensional architecture of presynaptic terminal cytomatrix. J. Neurosci. *27*, 6868–6877.

Stein, H., Spindler, S., Bonakdar, N., Wang, C., and Sandoghdar, V. (2017). Production of Isolated Giant Unilamellar Vesicles under High Salt Concentrations. Front. Physiol. *8*, 63.

Südhof, T.C. (2012). The presynaptic active zone. Neuron *75*, 11–25.

Südhof, T.C. (2013). Neurotransmitter release: the last millisecond in the life of a synaptic vesicle. Neuron *80*, 675–690.

Takamori, S., Holt, M., Stenius, K., Lemke, E.A., Grønborg, M., Riedel, D., Urlaub, H., Schenck, S., Brügger, B., Ringler, P., et al. (2006). Molecular anatomy of a trafficking organelle. Cell *127*, 831–846.

Tang, A.H., Chen, H., Li, T.P., Metzbower, S.R., MacGillavry, H.D., and Blanpied, T.A. (2016). A trans-synaptic nanocolumn aligns neurotransmitter release to receptors. Nature *536*, 210–214.

Um, J.W., and Ko, J. (2013). LAR-RPTPs: synaptic adhesion molecules that shape synapse development. Trends Cell Biol. *23*, 465–475.

Verhage, M., and Sørensen, J.B. (2008). Vesicle docking in regulated exocytosis. Traffic *9*, 1414–1424.

Wang, S.S.H., Held, R.G., Wong, M.Y., Liu, C., Karakhanyan, A., and Kaeser, P.S. (2016). Fusion Competent Synaptic Vesicles Persist upon Active Zone Disruption and Loss of Vesicle Docking. Neuron *91*, 777–791.

Wilhelm, B.G., Mandad, S., Truckenbrodt, S., Kröhnert, K., Schäfer, C., Rammner, B., Koo, S.J., Claßen, G.A., Krauss, M., Haucke, V., et al. (2014). Composition of isolated synaptic boutons reveals the amounts of vesicle trafficking proteins. Science *344*, 1023–1028.

Wong, M.Y., Liu, C., Wang, S.S.H., Roquas, A.C.F., Fowler, S.C., and Kaeser, P.S. (2018). Liprin-α3 controls vesicle docking and exocytosis at the active zone of hippocampal synapses. Proc. Natl. Acad. Sci. USA *115*, 2234–2239.

Wu, X., Cai, Q., Shen, Z., Chen, X., Zeng, M., Du, S., and Zhang, M. (2019). RIM and RIM-BP Form Presynaptic Active-Zone-like Condensates via Phase Separation. Mol. Cell *73*, 971–984.e5.

Wu, X., Cai, Q., Feng, Z., and Zhang, M. (2020). Liquid-Liquid Phase Separation in Neuronal Development and Synaptic Signaling. Dev. Cell *55*, 18–29.

Zeng, M., Shang, Y., Araki, Y., Guo, T., Huganir, R.L., and Zhang, M. (2016). Phase transition in postsynaptic densities underlies formation of synaptic complexes and synaptic plasticity. Cell *166*, 1163–1175.e12.

Zeng, M., Chen, X., Guan, D., Xu, J., Wu, H., Tong, P., and Zhang, M. (2018). Reconstituted postsynaptic density as a molecular platform for understanding synapse formation and plasticity. Cell *174*, 1172–1187.e16.

Zeng, M., Díaz-Alonso, J., Ye, F., Chen, X., Xu, J., Ji, Z., Nicoll, R.A., and Zhang, M. (2019). Phase Separation-Mediated TARP/MAGUK Complex Condensation and AMPA Receptor Synaptic Transmission. Neuron *104*, 529–543.e6.

Zhao, Y.G., and Zhang, H. (2020). Phase Separation in Membrane Biology: The Interplay between Membrane-Bound Organelles and Membraneless Condensates. Dev. Cell *55*, 30–44.

Ziv, N.E., and Garner, C.C. (2004). Cellular and molecular mechanisms of presynaptic assembly. Nat. Rev. Neurosci. *5*, 385–399.

Please cite this article in press as: Wu et al., Vesicle Tethering on the Surface of Phase-Separated Active Zone Condensates, Molecular Cell (2020), https://doi.org/10.1016/j.molcel.2020.10.029

CellPress

STAR★METHODS

KEY RESOURCES TABLE

REAGENT or RESOURCE	SOURCE	IDENTIFIER
Antibodies		
Synaptophysin 1, Monoclonal mouse purified IgG	Synaptic Systems	Cat#101 011
Synaptobrevin 2, Monoclonal mouse purified IgG	Synaptic Systems	Cat#104 211
VGLUT1, Polyclonal rabbit purified IgG	Synaptic Systems	Cat#135 302
PSD 95 PDZ domain, Monoclonal mouse purified IgG	Synaptic Systems	Cat#124 011
Na^+/K+ ATPase α-1, Monoclonal mouse purified IgG	Millipore	Cat# 05-369
SDHA, Monoclonal mouse purified IgG	Abcam	Cat#ab14715
Goat Anti-Mouse IgG (H + L)-HRP Conjugate	Bio-Rad	Cat #1706516
Goat Anti-Rabbit IgG (H + L)-HRP Conjugate	Bio-Rad	Cat# 1706515
Bacterial and Virus Strains		
Escherichia coli BL21 (DE3) cells	Invitrogen	Cat#C600003
DH10Bac cells	Thermo Fisher	Cat#10361012
Chemicals, Peptides, and Recombinant Proteins		
Alexa Fluor 647 NHS Ester	Thermo Fisher	Cat#A20106
iFluor 405 NHS Ester	AAT Bioquest	Cat#1021
iFluor 488 NHS Ester	AAT Bioquest	Cat#1023
Cy3 NHS Ester	AAT Bioquest	Cat#271
Cy5 NHS Ester	AAT Bioquest	Cat#280
DiO	AAT Bioquest	Cat#22066
DiI	AAT Bioquest	Cat#22102
DiD	AAT Bioquest	Cat#22054
18:1 Cy5 PE	Avanti Polar Lipids	Cat#810335C
16:0-18:1 PC (POPC)	Avanti Polar Lipids	Cat#850457P
18:1 PS (DOPS)	Avanti Polar Lipids	Cat#840035P
18:1 (Δ9-Cis) PE (DOPE)	Avanti Polar Lipids	Cat#850725P
18:1 PI(4,5)P2	Avanti Polar Lipids	Cat#850155P
18:1 DGS-NTA(Ni)	Avanti Polar Lipids	Cat#790404P
18:1 PEG5000 PE	Avanti Polar Lipids	Cat#880230P
Cholesterol	Echelon lipids	Cat#L-6012
FuGENE® HD Transfection Reagent	Promega	Cat#E2311
Cocktail protease inhibitor	Bimake	Cat#B14002
PMSF	Sigma	Cat#P7626
Pepstatin A	Peptide Institute Inc	Cat#4397
Uranyl acetate	Electron Microscopy Sciences	Cat#22400
Sodium cholate	Sigma	Cat#27029
Sucrose	Merck	Cat#107651
HEPES	Roth	Cat#6763.3
Glycine	Merck	Cat#104201

(*Continued on next page*)

Please cite this article in press as: Wu et al., Vesicle Tethering on the Surface of Phase-Separated Active Zone Condensates, Molecular Cell (2020), https://doi.org/10.1016/j.molcel.2020.10.029

Continued

REAGENT or RESOURCE	SOURCE	IDENTIFIER
trypsin	Sigma	Cat#T9201
aprotinin	Sigma	Cat#A1153
PVA	Sigma	Cat#363065
PEG8000	Sigma	Cat#81272
μ-Plate 96 well	ibidi	Cat#89621
SuperSignal West Pico PLUS Chemiluminescent Substrate	Thermo Fischer	Cat#34579
RIM1α-PAS (aa 481-1097)	Wu et al., 2019	N/A
RIM1α-S (aa 871-1097)	Wu et al., 2019	N/A
RIM1α-N-LPETGG (aa 1-474-LPETGG)	Wu et al., 2019	N/A
RIM1α-PASB (aa 481-1334)	Wu et al., 2019	N/A
Sortase A-ΔN59 (aa 60-206)	Wu et al., 2019	N/A
RBP2-(SH3)3 (aa 178-252+844-1040)	Wu et al., 2019	N/A
RBP2-3rd SH3 (aa 966-1040)	Wu et al., 2019	N/A
VGCC-CT (aa 2151-2327)	Wu et al., 2019	N/A
mEGFP-synapsin-FL (aa 1-706)	This paper	N/A
mCherry-synapsin-FL (aa 1-706)	This paper	N/A
Synapsin-CD (aa 110-657)	This paper	N/A
ITSN (aa 740-1214)	This paper	N/A
PSD95-PSG (aa 309-724)	Zeng et al., 2016	N/A
SynGAP-CC-PBM (aa 1147-1308)	Zeng et al., 2016	N/A
ELKS1 (aa 141-660 + 938-948)	This paper	N/A
ELKS2 (aa 137-664 + 967-977)	This paper	N/A
HRV-3C protease	This paper	N/A
TEV protease	This paper	N/A
Deposited Data		
Original imaging data - Mendeley Data	This paper	https://dx.doi.org/10.17632/9d7y8tz98g.1
Experimental Models: Cell Lines		
GIBCO® Sf9 cells	Thermo Fisher	Cat#12659017
Recombinant DNA		
pET-32a	Novagen	Cat#69015-3
pFastBac	Thermo Fisher	Cat#10712024
32m3c-RIM1α-PAS (aa 481-1097)	Wu et al., 2019	N/A
32m3c-RIM1α-S (aa 871-1097)	Wu et al., 2019	N/A
32m3c-RIM1α-N-LPETGG (aa 1-474-LPETGG)	Wu et al., 2019	N/A
32m3TEV-RIM1α-PASB (aa 481-1334)	Wu et al., 2019	N/A
Sortase A-ΔN59 (aa 60-206)	Wu et al., 2019	N/A
m3c-RBP2-(SH3)3 (aa 178-252+844-1040)	Wu et al., 2019	N/A
32m3c-RBP2-3rd SH3 (aa 966-1040)	Wu et al., 2019	N/A
32mTEV-VGCC-CT (aa 2151-2327)	Wu et al., 2019	N/A
pFastBac-mEGFP-synapsin-FL (aa 1-706)	This paper	N/A
pFastBac-mCherry-synapsin-FL (aa 1-706)	This paper	N/A
32m3c-Synapsin-CD (aa 110-657)	This paper	N/A
32m3c-ITSN (aa 740-1214)	This paper	N/A
m3c-PSD95-PSG (aa 309-724)	Zeng et al., 2016	N/A
32m3c-SynGAP-CC-PBM (aa 1147-1308)	Zeng et al., 2016	N/A
32m3c-ELKS1 (aa 141-660 + 938-948)	This paper	N/A

(*Continued on next page*)

Please cite this article in press as: Wu et al., Vesicle Tethering on the Surface of Phase-Separated Active Zone Condensates, Molecular Cell (2020), https://doi.org/10.1016/j.molcel.2020.10.029

Continued

REAGENT or RESOURCE	SOURCE	IDENTIFIER
32m3c-ELKS2 (aa 137-664 + 967-977)	This paper	N/A
HRV-3C protease	Wu et al., 2019	N/A
TEV protease	Wu et al., 2019	N/A
Software and Algorithms		
ImageJ	NIH	https://imagej.nih.gov/ij/
Prism	GraphPad	https://www.graphpad.com/scientific-software/prism/
AIDA Image Analysis software	Elysia-Raytest	https://www.elysia-raytest.com/en/cataloglight/aida-image-analysis-software~8708faa6-41a1-4827-881b-2671ec1c824d
Other		
Superdex 75 26/60	GE Healthcare	Cat#28-9893-34
Superdex 200 26/60	GE Healthcare	Cat#28-9893-36
HiTrap desalting column	GE Healthcare	Cat#29-0486-84
NanoDrop 2000/2000c Spectrophotometers	Thermo Fisher	Cat#ND-2000
Controlled-pore glass bead (CPG-3000, glycerol coated)	LGC Biosearch GmbH	Cat#BG6-5002

RESOURCE AVAILABILITY

Lead contact

Further information and requests for resources and reagents should be directed to and will be fulfilled by the Lead Contact, Mingjie Zhang (mzhang@ust.hk).

Materials availability

This study did not generate new unique reagents.

Data and code availability

All original imaging data of our study have been deposited to Mendeley Data with the link of: https://dx.doi.org/10.17632/9d7y8tz98g.1

EXPERIMENTAL MODEL AND SUBJECT DETAILS

Bacterial strain

Escherichia coli BL21-CodonPlus(DE3)-RIL cells (Agilent #230245) were used in this study to express all the recombinant proteins except for synapsin. Cells were cultured in LB medium supplemented with necessary antibiotics.

DH10Bac cells (ThermoFisher #10361012) were used for recombinant bacmid production.

Cell line

GIBCO® Sf9 cells (ThermoFisher #12659017) were used in this study to express synapsin. Cells were cultured in Sf-900 III SFM medium (ThermoFisher #12658027).

METHOD DETAILS

Genes and constructs

Rat *RIM1*α (NCBI reference sequence: XM_017596673.1) and *RIM-BP2* (NCBI reference sequence: XM_017598284.1) constructs were gifts from Dr. Pascal S. Kaeser at Harvard Medical School. Rat *ELKS1* (NCBI Reference Sequence: NM_170788.2), mouse *ELKS2* (NCBI Reference Sequence: XR_001781113.2), mouse *synapsin Ia* (NCBI Reference Sequence: NM_013680.4) and mouse cytoplasmic tail of N-type *VGCC* $\alpha 1$ subunit (NCBI Reference Sequence: NP_001035993.1) were amplified from rat and mouse brain libraries. Human *Intersectin 1* was purchased from Addgene (Addgene #47395, GenBank: AF114487.1).

Please cite this article in press as: Wu et al., Vesicle Tethering on the Surface of Phase-Separated Active Zone Condensates, Molecular Cell (2020), https://doi.org/10.1016/j.molcel.2020.10.029

Constructs of RIM, RIM-BP, and VGCC were generated in our previous work (Wu et al., 2019). ELKS1, ELKS2, synapsin-CD, and Intersectin (ITSN) were amplified by standard PCR and inserted into a modified pET-32a vector with an N-terminal Trx-His_6 tag and an HRV-3C protease cleavage site. Full-length synapsin was cloned into a modified pFastBac vector with an N-terminal EGFP or mCherry and a His_6-tag. All constructs were confirmed by DNA sequencing.

Protein expression and purification

All proteins except for full-length synapsin were expressed in *Escherichia coli* BL21-CodonPlus(DE3)-RIL cells (Agilent Technologies). The cells were growing in LB medium at 37°C until OD_{600} reached ~0.6, then 0.25 mM IPTG was added into the cultures to induce the protein expression at 16°C overnight. Recombinant proteins were extracted by high pressure homogenizer and purified using a Ni^{2+}-NTA (GE Healthcare) affinity column followed by size exclusion chromatography using Superdex 200 26/60 (GE Healthcare) with a buffer containing 50 mM Tris pH 8.2, 100 mM NaCl, 1 mM DTT, 1 mM EDTA (or 50 mM Tris pH 8.2, 300 mM NaCl, 1 mM DTT, 1 mM EDTA for RIM1α). The affinity tag was cleaved by HRV-3C protease at 4°C overnight and then removed by another step of Superdex 200 26/60 size exclusion chromatography with the column buffer of 20 mM HEPES pH 7.5, 100 mM NaCl, 1 mM TCEP or 20 mM HEPES pH 7.5, 300 mM NaCl, 1 mM TCEP for RIM1α. This column buffer was also used as the reaction buffer throughout this study unless otherwise specified.

Sortase-mediated protein ligation

As described in our previous work (Wu et al., 2019), the full-length RIM was generated by sortase ligation. Purified RIM-N(1-474) with a "LPETGG"-tag at the C terminus, GGG-RIM-PASB and sortase Δ59 were mixed at a 2:1:1 molar ratio. The ligation reaction was initiated by addition of 10 mM $CaCl_2$ at room temperature for 2 h. The ligated RIM-FL was separated from unreacted substrates and enzymes by Superdex 200 26/60 size exclusion chromatography in a buffer containing 20 mM HEPES pH 7.5, 300 mM NaCl, 1 mM TCEP.

Synapsin full-length expression and purification

Synapsin was first cloned in the pFastBac vector and then transformed into the DH10Bac to generate the recombinant bacmid. The bacmid was transfected into sf9 cells with FuGENE® HD Transfection Reagent (Promega # E2311) to produce the first generation of baculovirus (P1), then the P1 was used to prepare P2 and P3. Typically, a 500ml culture in a 2L flask was grown at 27°C with shaking at 100 rpm. The culture was then infected by moderate amount (~0.5% volume of the culture) of P3 at a cell density of $1.5*10^6$ cells/ml and cultured for another 64h under the same culture condition. Cells were harvested by centrifugation and resuspended with binding buffer containing 50 mM Tris pH 8.2, 1000 mM NaCl, 5 mM imidazole, 1x cocktail protease inhibitor (Bimake #B14002). Then the cells were lysed by high pressure homogenizer and proteins were purified using a Ni^{2+}-NTA (GE Healthcare) affinity column followed by size exclusion chromatography using Superdex 200 26/60 (GE Healthcare) with the reaction buffer as the column buffer.

Protein labeling with fluorophore

The iFluor 405/iFluor 488/Cy3/Cy5 NHS easter (AAT Bioquest) and Alexa 647 NHS ester (ThermoFisher) fluorophores were each dissolved in DMSO at 10 mg/ml. Purified proteins were kept in the reaction buffer at a concentration of 5~10 mg/ml. The fluorophores were added into the protein solution in a 1:1 molar ratio. The reaction was proceeded with shaking at room temperate for 1 h in dark. After quenching by 200 mM Tris pH 8.2, labeled proteins were exchanged into the reaction buffer using a HiTrap desalting column (GE Healthcare). Fluorescence labeling efficiency was determined using Nanodrop 2000 (ThermoFisher #ND-2000). The final labeling of each protein by a specific fluorophore was adjusted to 1% by mixing labeled protein with unlabeled at a 1:99 ratio.

Small Uni-lamellar Vesicle (SUV) preparation

Lipids (from Avanti Polar Lipids) were dissolved in chloroform and stored at −20°C. Lipids were mixed at desired molar ratios (POPC-SUV: 98% POPC + 2% dye; DOPS-SUV: 78% POPC + 20% DOPS + 2% dye; PIP2-SUV: 76% POPC + 20% DOPS + 2% PI(4,5)P2 + 2% dye; Cholesterol-SUV: 44.7% Cholesterol + 53.3% * (46% POPC + 40% DOPE + 12% DOPS + 2% PI(4,5)P2) + 2% dye (DiO (ThermoFisher), DiI (ThermoFisher), or Cy5-PE (Avanti Polar Lipids)) in a 2 mL glass vial with glass pipette and dried under nitrogen gas stream, followed by at least 1 h vacuum to ensure removal of residual chloroform. The lipid mixture cake was resuspended by the reaction buffer supplemented with 1% sodium cholate (Sigma #27029). Lipids completely dissolved in this detergent environment should be transparent. The dissolved lipid mixture was subjected to a HiTrap desalting column (GE Healthcare) with the reaction buffer, SUVs were formed during the detergent removal process. The concentration of SUVs was estimated by measuring the fluorophore concentration using Nanodrop 2000 (ThermoFisher #ND-2000).

Imaging

All protein aliquots were centrifuged at 16,000 *rcf.* for 10 min at 4°C to remove potential precipitations prior to imaging. Proteins were directly mixed to reach desired concentrations. Normally the working concentration was 5 μM for each protein and 10 μM for SUV (lipid concentration). Imaging buffer was the reaction buffer (20 mM HEPES pH 7.5, 100 mM NaCl, 1 mM TCEP) unless otherwise specified. For synapsin phase separation, 3% PEG8000 (Sigma #81272) was supplemented in the reaction buffer (Milovanovic et al., 2018).

Please cite this article in press as: Wu et al., Vesicle Tethering on the Surface of Phase-Separated Active Zone Condensates, Molecular Cell (2020), https://doi.org/10.1016/j.molcel.2020.10.029

A Zeiss LSM 880 confocal microscope with a 63x oil lens was used as the default imaging microscope. Each mixture was injected into a home-made chamber composed of a coverslip and a glass slide assembled with one-layer of double-sided tape. The chamber was sealed by vacuum grease after sample loading. For imaging GUVs and assays require sample injections (Figure 1H; Figure S5C), μ-Plate 96 well micro-plates (ibidi #89621) were used. DIC and fluorescent images were captured on a Nikon Ni-U upright fluorescence microscope at room temperature.

SUV coating efficiency and corresponding protein intensity comparison

All confocal images of SUV-coated RIM/RIM-BP droplets were captured under the identical condition (e.g., the laser power, detector gain, resolution, scanning speed, etc.). All images were taken in one single imaging session. At least 10 independent images for each group were recorded. Images were analyzed with the ImageJ software. Droplets with diameter ranging from 20∼50 pixels (2.64∼6.59 μm) were used for analysis.

Sedimentation assay

The sedimentation assay was performed as described before (Wu et al., 2019). Briefly, a total volume of 40 μL protein mixture was incubated at room temperature (22°C) for 10 min, followed by 5 min centrifugation at 16,873 g at 22°C. The supernatant and pellet fractions were separated, the pellet was resuspended with the assay buffer to the same volume (40 μL). Proteins in the supernatant and pellet fractions were analyzed by SDS-PAGE.

Fluorescence recovery after photobleaching (FRAP) assay

FRAP experiments were performed on a Zeiss LSM 880 confocal microscope at room temperature. A square region (R1) was selected. A neighboring region (R2) with the same size containing another droplet with a similar size as the one selected for R1 was recorded for fluorescence intensity correction, and a third region (R3) in the background with the same size was also recorded for background subtraction. The size of the region keeps the same for each experiment. For RIM/RIM-BP coated by SUV (Figure 1E), the side length was 30 pixels; for RIM/RIM-BP on GUV (Figure S4A), the side length was 5 pixels; for RIM/RIM-BP encapsulated by synapsin (Figure S6A), the side length was 10 pixels; for synapsin enveloping RIM/RIM-BP, the side length was 20 pixels. The pixel size was 0.13 μm. Cy3 labeled RIM-BP and EGFP-synapsin were photobleached by 561 nm and 488 nm laser beams, respectively, at the 100% power with 30 iterative pulses. Each data point represented the averaged signal of six droplets. All experiments were completed within 2 h after initiation of the phase separation. For data analysis, the intensity at the pre-bleach point was normalized to 100%, and the intensity right after the bleaching was set to 0%. Data were expressed as mean ± SD.

Negative staining

Negative stain analysis was performed using 300 mesh carbon coated copper grids (EMResolutions). Grids were glow discharged for 30 s at 15 mA using an easiGlow glow discharger (PELCO). A 5 μL drop of 15 ng/μl SUV was applied onto the grid and incubated for 2 min. The sample was then quickly blotted away and 5 μL drop of 2% uranyl acetate solution was applied for 30 s before blotting to complete dryness. Negative stain images were collected using a Talos L120C transmission electron microscope (ThermoFisher Scientific) operating at 120 kV. Images were recorded using a 4k × 4k BM-Ceta camera (ThermoFisher Scientific) at a nominal magnification of 36,000 × corresponding to 4.03 Å/pixel at the specimen level.

Cryo-EM imaging

Cryo-EM imaging was performed using R2/2 holey carbon (300 copper mesh) grids (QUANTIFOIL). Grids were glow discharged for 90 s at 15 mA using an easiGlow glow discharger (PELCO). Protein-SUV mixtures were prepared at the specified final concentrations and incubated at room temperature for 30 min before grid application. A 3 μL drop of the protein-SUV mixture was applied onto freshly glow-discharged grids and incubated for 2 min at 21°C with 100% humidity in a Vitrobot Mark IV (ThermoFisher Scientific). Grids were blotted from both sides for 3 s and plunge-frozen in liquid ethane. Images were collected using a Glacios transmission electron microscope (ThermoFisher Scientific) operating at 200 kV. Images were recorded using a 4k × 4k Falcon 3 camera (ThermoFisher Scientific) at a nominal magnification of 56,000 × corresponding to 2.6 Å/pixel at the specimen level.

Synaptic Vesicle (SV) purification

Synaptic vesicles were isolated according to previous publications from rat brain (Nagy et al., 1976; Takamori et al., 2006). Briefly, 20 rat brains were homogenized in 240 mL ice-cold sucrose buffer (320 mM sucrose, 4 mM HEPES-KOH, pH 7.4 supplemented with 0.2 mM PMSF and 1 mg/ml pepstatin A). Cellular debris was removed by centrifugation (10 min at 900 g, 4°C) and the resulting supernatant was further centrifuged for 10 min at 12,000 g, 4°C. The pellet containing synaptosome was washed once by carefully resuspending it in sucrose buffer and further centrifuged for 15 min at 14,500 g, 4°C (the brown bottom part in the center of the pellet, enriched in mitochondria and peroxisomes, was avoided during resuspension). Synaptosomes were lysed by hypo-osmotic shock (by addition of 9 volumes distilled water, buffered with 5 mM HEPES-NaOH, pH 7.4 and supplemented with 0.2 mM PMSF and 1 mg/ml pepstatin A, followed by homogenization). Free, released SVs were obtained after centrifugation of the lysate for 20 min at 14,500 g, 4°C. The supernatant containing the SVs was further ultracentrifuged for 2 h at 230,000 g, 4°C, yielding a crude synaptic vesicle pellet. SVs were purified by resuspending the pellet in 40 mM sucrose followed by centrifugation for 3 h at 110,880 g on a continuous

Please cite this article in press as: Wu et al., Vesicle Tethering on the Surface of Phase-Separated Active Zone Condensates, Molecular Cell (2020), https://doi.org/10.1016/j.molcel.2020.10.029

sucrose density gradient (50–800 mM sucrose). SVs were collected from the gradient and subjected to size-exclusion chromatography on controlled pore glass beads (300 nm diameter), equilibrated in glycine buffer (300 mM glycine, 5 mM HEPES, pH 7.40, adjusted using KOH), to separate synaptic vesicles from residual larger membrane contaminants. SVs were pelleted by centrifugation for 2 h at 230,000 g, 4°C and resuspended in 400 μL sucrose buffer by homogenization before being aliquoted into single-use fractions (20 μL each) and snap frozen in liquid N2 and transfer to −80°C for long time storage.

SV characterization

Purified SVs were examined by negative staining EM imaging and immunoblotting. For negative staining, all the operations were same as SUV except that the sample concentration was 20 ng/μl. For immunoblotting, 2 μg of protein of the respective fractions was used for detection by standard immunoblot technique. Samples were separated on SDS-polyacrylamide minigels and blotted onto nitrocellulose membranes. The blots were developed using secondary antibodies (anti-mouse and anti-rabbit IgG, respectively) coupled to horseradish-peroxidase and an enhanced luminol-based chemiluminescent substrate. The signals were recorded on a Fujifilm LAS-100 cooled CCD instrument using Image Reader and Raytest Aida image analysis software. Primary and secondary antibodies were diluted at the specific concentration of 1:1000 and 1:2000, respectively. The antibodies used were obtained from the following sources (M, mouse monoclonal antibody, R, rabbit polyclonal serum): Synaptic Systems: synaptophysin 1 (M), synaptobrevin 2 (M), VGLUT1 (R) and PSD95 (M). Millipore: Na^+/K+ ATPase α1 (M). Abcam: SDHA (M).

Labeling SVs with fluorescent dyes

The SV staining procedure was optimized based on the previously method (Kiessling et al., 2013). Briefly, an aliquot of SV (20 μL at 2.5 mg/ml) stored at −80°C was thawed on ice. The aliquot was centrifuged at 16,900 *rcf.* for 10 min at 4°C to remove precipitates. The supernatant was recovered for labeling. For labeling SVs with the hydrophobic dye DiO (AAT Bioquest #22066), 10 μL of the dye dissolved chloroform (1 mg/ml) was dried under nitrogen gas stream in a clean glass vial followed by vacuuming for 1 h to remove residual chloroform. Then resuspend the dried dye with 20 μL SV buffer (20 mM HEPES pH 7.5, 100 mM KCl) with intense vortex followed by 20 μL SV supernatant with gentle vortex. For labeling SVs with the amphiphilic dye DiD (AAT Bioquest #22054), the dye was dissolved directly in the SV buffer, and the mixture was centrifuged at 16,900 *rcf.* for 10 min. The supernatant containing the saturation concentration of DiD (estimated to ∼0.1 mg/ml or less) was recovered for SV labeling. Equal volumes of DiD and the SV supernatant (20 μl) were mixed with gentle pipetting. For both of the SV labeling methods, the SV/dye mixtures were incubated in a 37°C water bath for 30 min followed by 30 min centrifugation at 16,900 *rcf.* at 4°C. The supernatant was recovered and another 60 μL of the SV buffer was added to bring the total sample volume to 100 μL (stock concentration: 0.5 mg/ml). The labeled SVs were placed on ice and used within two days.

Trypsin digestion of SVs

A dye labeled SV solution at 0.5 mg/ml was mixed with 0.25% volume of the trypsin stock (Sigma # T9201, 10 mg/ml in 50 mM acetic acid), and the reaction was lasted for 3 h at room temperature. The digestion reaction was stopped by adding 0.25% volume of an aprotinin (Sigma #A1153) stock solution (10 mg/ml in 50 mM MES pH 6.5, 150 mM NaCl) followed by incubation at room temperature for another 1 h.

Giant Uni-lamellar Vesicle (GUV) preparation and imaging

Polyvinyl alcohol (PVA, MW 146,000∼186,000, Sigma #363065) assisted GUV preparation was adopted as described previously (Stein et al., 2017). Briefly, PVA was dissolved in ddH_2O at 10% (m/v) concentration. An aliquot of 20 μL of PVA was spread on a glass slide to form a uniform thin layer. The PVA-coated slide was dried at 40∼50°C for ∼30 min. A lipid mixture (93% POPC + 5% DGS-NTA + 2% Cy5-PE) was dissolved in chloroform at 1 mg/ml concentration in a glass vial. An aliquot of 20 μL of this lipid mixture was spread on the dried PVA layer using a glass pipette. Chloroform was evaporated immediately after spreading, the dried glass slide was placed in vacuum for at least another 1 h to remove residual chloroform. An O-ring was glued on to the glass slide. Then 200 μL of GUV preparation buffer (200 mM sucrose, 20 mM Tris pH 8.2, 50 mM NaCl) was injected to the inside of the O-ring followed by 1 h incubation at room temperature in dark. The GUVs solution inside the O-ring was withdrawn and kept on ice. Prepared GUV stock was used within two days. Typically, the GUV solution was diluted with PBS by 20-folds for each experiment and in μ-Plate 96 well plates (ibidi #89621) for imaging.

For tethering VGCC-CT to GUVs, VGCC-CT at 0.5 μM was incubated with the GUV solution for 30 min. RIM and RIM-BP (0.5 μM) was added to the VGCC-CT-tethered GUV solution to assay the RIM/RIM-BP droplet formation on GUVs. For the SUV tethering assay, another 5 μM DOPS-SUVs were added. Finally, mCherry-synapsin and ITSN (1 μM each supplemented with 2% PEG8000) was added to the above mixture to reconstitute the reserve and tethered pools of SUVs in the synapsin and RIM/RIM-BP co-condensate system.

QUANTIFICATION AND STATISTICAL ANALYSIS

For SUV imaging, a total of 10 images with 10 randomly selected droplets from each image (i.e., a total of 100 droplets) in each group were pooled together for quantification. Once a droplet was selected, for SUV intensity, a horizontal line scan across the center of the

Please cite this article in press as: Wu et al., Vesicle Tethering on the Surface of Phase-Separated Active Zone Condensates, Molecular Cell (2020), https://doi.org/10.1016/j.molcel.2020.10.029

droplet was generated and peak intensities on the edge of the droplet were averaged to get one data point for each droplet. For protein intensity, a smaller circular area fitting the size of a droplet was used to measure the mean intensity of the droplet. Number of droplets, distributions, and deviations are reported in the figures and corresponding figure legend. Data were expressed as mean ± SD. ****, $p < 0.0001$; ns, not significant, $p > 0.05$ using one-way ANOVA with Tukey's multiple comparisons test. Statistical analysis was performed in GraphPad Prism.

For sedimentation assay, three repeats were performed for each group. The SDS-PAGE was analyzed by ImageJ, data were expressed as mean ± SD ns, not significant, $p > 0.05$; ****, $p < 0.0001$ using one-way ANOVA with Tukey's or Dunnett's multiple comparisons test accordingly. Statistical analysis was performed in GraphPad Prism.

For cyro-EM quantification, a total of 8 images from each group were analyzed. We defined a layer with thickness of 40 nm (a value comparable to the diameter of the SUVs) from the edge of the protein droplets as the condensate surface (S1), and the surrounding area within the EM grid hole as the dilute solution area (S2). We counted the number of SUVs in the surface area (N1) and in the solution area (N2). Two parameters were used to measure the coating efficiency. (1) SUV density on the surface of protein droplets, which is defined as N1/S1; (2) SUV enrichment fold, which is defined as (N1/S1)/((N1+N2)/(S1+S2)). ns, not significant, $p > 0.05$; **, $p < 0.005$; ****, $p < 0.0001$ using one-way ANOVA with Tukey's multiple comparisons test. Statistical analysis was performed in GraphPad Prism.

For SV coating efficiency comparison, similar to SUV coating experiment except for the analyzed number of droplets. A total of 5 images with 10 randomly selected droplets from each image (i.e., a total of 50 droplets) in each group were analyzed. Number of droplets, distributions, and deviations are reported in the figures and corresponding figure legend. Data were expressed as mean ± SD. ****, $p < 0.0001$ using one-way ANOVA with Dunnett's multiple comparisons test. Statistical analysis was performed in GraphPad Prism.

For quantifications in Figures 4 and 5, three independent repeats were performed. Multiple images were captured for each repeat, the total number of GUVs was counted as N(GUV) (N(GUV) > 50). Among them, the number of GUVs with RIM/RIM-BP phase separation occurred was counted as $N(GUV_{phase})$. Then the proportion of GUV with RIM/RIM-BP phase separation was calculated by $N(GUV_{phase})/N(GUV)$.

All quantification and statistics analyses are also included in the relevant figure legends.